



## A review on mechanistic understanding of MnO<sub>2</sub> in aqueous electrolyte for electrical energy storage systems

Jaewook Shin, Joon Kyo Seo, Riley Yaylian, An Huang & Ying Shirley Meng

To cite this article: Jaewook Shin, Joon Kyo Seo, Riley Yaylian, An Huang & Ying Shirley Meng (2019): A review on mechanistic understanding of MnO<sub>2</sub> in aqueous electrolyte for electrical energy storage systems, International Materials Reviews, DOI: [10.1080/09506608.2019.1653520](https://doi.org/10.1080/09506608.2019.1653520)

To link to this article: <https://doi.org/10.1080/09506608.2019.1653520>



Published online: 20 Aug 2019.



Submit your article to this journal [↗](#)



Article views: 31



View related articles [↗](#)



View Crossmark data [↗](#)

# A review on mechanistic understanding of $\text{MnO}_2$ in aqueous electrolyte for electrical energy storage systems

Jaewook Shin <sup>a</sup>, Joon Kyo Seo <sup>a,b</sup>, Riley Yaylian <sup>a,b</sup>, An Huang <sup>a,b</sup> and Ying Shirley Meng<sup>a</sup>

<sup>a</sup>Department of NanoEngineering, University of California, San Diego, La Jolla, CA, USA; <sup>b</sup>Materials Science & Engineering Program, University of California, San Diego, La Jolla, CA, USA

## ABSTRACT

The demand for the large-scale storage system has gained much interest. Among all the criteria for the large-scale electrical energy storage systems (EESSs), low cost ( $\$ \text{ k Wh}^{-1}$ ) is the focus where  $\text{MnO}_2$ -based electrochemistry can be a competitive candidate. It is notable that  $\text{MnO}_2$  is one of the few materials that can be employed in various fields of EESSs: alkaline battery, supercapacitor, aqueous rechargeable lithium-ion battery, and metal-air battery. Yet, the technology still has bottlenecks and is short of commercialisation. Discovering key parameters impacting the energy storage and developing systematic characterisation methods for the  $\text{MnO}_2$  systems can benefit a wide spectrum of energy requirements. In this review, history, mechanism, bottlenecks, and solutions for using  $\text{MnO}_2$  in the four EESSs are summarised and future directions involving more in-depth mechanism studies are suggested.

## ARTICLE HISTORY

Received 28 February 2018  
Accepted 28 July 2019

## KEYWORDS

Electrical energy storage systems; alkaline battery; lithium-ion battery; supercapacitor; metal-air battery

## Introduction

A large-scale energy storage system in a grid-scale power generator provides a substantial benefit to the electric power grid by lowering the need for generating constant and excessive power [1]. Because the power consumption fluctuates throughout the day, the excess power is wasted without the energy storage systems to level the load. The load levelling is to store and utilise the excess energy when needed. Currently, less than 2.5% of the total electric power delivered in the United States uses energy storage systems [2]; the need for a large-scale energy storage system is evident. As an energy storage device, the pumped hydroelectric system is the dominant system, however, it suffers from a geometric constraint and a low efficiency [3]. To gain flexible installation with higher efficiency, the electrical energy storage system (EESS) is favoured. While hydroelectricity stores the energy in a form of water displacement and converts it to electricity, the EESS stores the energy in the form of electricity. The stored energy can be directly utilised to the grid.

One of the major difficulties in installing an EESS is the cost of the materials. For a large-scale EESS, the material cost has to stay low and  $\text{MnO}_2$  is a promising candidate in terms of the cost. Manganese is the 12th most abundant element in the Earth's crust [4]; it is a significant component in soil [5–7]; thus, making it one of the cheapest materials available. However,  $\text{MnO}_2$  has intrinsic issues that hinder its rechargeable application. Since EESS is in dire need of improvement, we propose the  $\text{MnO}_2$  system to study. There has been

an extensive history of academic and industrial research on  $\text{MnO}_2$ . Academic approach and understanding of the  $\text{MnO}_2$  in EESS research are summarised and discussed in this review.

The electrochemical activities of  $\text{MnO}_2$  have been reported for more than a century. The ancient  $\text{MnO}_2$  system deserves the spotlight because of its complexity. The recent development of characterisation techniques and knowledge broadened the understanding of the  $\text{MnO}_2$  system and left room to improve in addition to the study done over the last few decades. First of all,  $\text{MnO}_2$  does not refer to a single material. It is necessary to understand that there are a few polymorphs of  $\text{MnO}_2$  and they should be considered differently [8,9]. Due to the difference in the crystal structure of the  $\text{MnO}_2$ , a redox reaction kinetic is completely disparate [10]. There are six polymorphs of manganese dioxide this review discusses in detail: (1)  $\alpha$ - $\text{MnO}_2$  ( $2 \times 2$  tunnel or hollandite), (2)  $\beta$ - $\text{MnO}_2$  ( $1 \times 1$  tunnel or pyrolusite), (3) R- $\text{MnO}_2$  ( $2 \times 1$  tunnel or Ramsdellite), (4)  $\gamma$ - $\text{MnO}_2$  (mix of  $2 \times 1$  and  $1 \times 1$  tunnels or nsutite), (5)  $\delta$ - $\text{MnO}_2$  (layered or birnessite), and (6)  $\lambda$ - $\text{MnO}_2$  (3-dimensional pores or spinel) (Figure 1). The polymorphs have distinctive atomic arrangements that result in various types of pores or tunnels within the crystal structure. Due to the distinctive crystal structure, the selectivity towards different ions or electron transfer kinetics is immense. Since most EESS utilises ions in the electrolyte and electron transfer kinetics on the electrode surface, it is expected that the crystal structures and the applications are closely related.

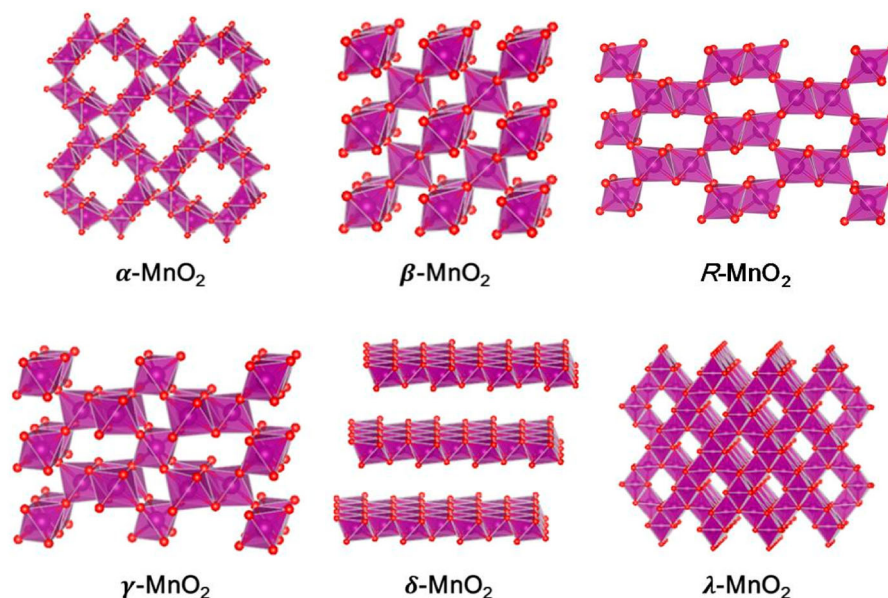


**Figure 1.** Crystal structures of  $\text{MnO}_2$  polymorphs (Mn: magenta and O: red). The structure of  $\gamma\text{-MnO}_2$  consists of an intergrowth between  $1 \times 1$  and  $2 \times 1$  tunnels. The ratio of  $1 \times 1$  tunnel over  $1 \times 1$  and  $2 \times 1$  tunnels is called Pr ( $0\% < \text{Pr} < 100\%$ ) [11]. The shown  $\gamma\text{-MnO}_2$  compound has Pr = 50%. Water molecules and guest cations are omitted for clarity.

There are four major types of EESS in which  $\text{MnO}_2$  has been adopted: alkaline battery, lithium-ion battery (LIB), supercapacitor, and metal-air battery (MAB). All EESS in discussion focuses on aqueous electrolyte systems because of their low cost compared to their counterpart, organic electrolyte systems. Great interest in these systems has exponentially grown over the years (Figure 2(a)). Especially, the alkaline battery system has the longest history of the four systems with more academic research papers published than the other three systems. On the other hand, although the supercapacitor, LIB, and MAB systems have a shorter history, a growing number of papers are being published recently. Gathering the large literature, the four EESS have distinctive mechanisms, which fill different areas on the Ragone plot (Figure 2(b)) can be learned. The alkaline battery has high energy, but low power, whereas the supercapacitor has high power and low energy. The LIB performances sit in between the two and the metal-air has a wide range of energy, but narrow power. In the large-scale energy storage, the power required by the consumers fluctuates in seconds to hours. It is vital to have complimentary EESS to compensate for the wide range fluctuation. For instance, an alkaline battery with low power but high energy is favoured in the hour-range of fluctuation and a supercapacitor with high power but low energy is suitable for the second-range of fluctuation. In the real world with dynamic ranges of the fluctuation, the varying EESS performances will complement each other. In this review, the performance, mechanism, bottleneck, and solutions of  $\text{MnO}_2$  in the four EESS are discussed.

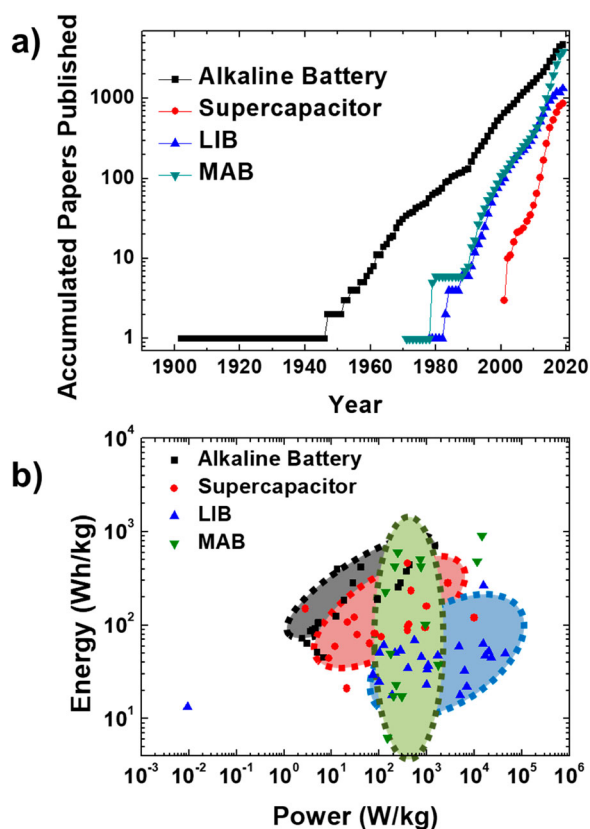


**Figure 2.** (a) Accumulated papers (articles and review) published on various EESS systems. Source: Web of Science database. (b) A Ragone plot comparing alkaline battery, LIB, supercapacitor, and a MAB that utilise manganese dioxide. Source: Web of Science database. Data is updated in June 2019.

### Alkaline battery

#### $\text{MnO}_2$ in alkaline battery

Utilising  $\text{MnO}_2$  in an electrochemical system among the four EESS, an alkaline battery has the longest

history. Since it was first commercialised in the 1950s, the  $\text{MnO}_2/\text{Zn}$  alkaline chemistry has been widely applied to operate household goods as well as small portable devices [12]. Recently, adopting alkaline batteries into grid-scale EESS is emerging especially in load levelling and stabilising intermittent renewable energy from solar and wind power [13].  $\text{MnO}_2$  in alkaline batteries has several advantages: low cost, high energy density, and safety. Specifically, the  $\text{MnO}_2/\text{Zn}$  alkaline battery has a capital cost of \$ 10–65 per kWh [14–16], the theoretical energy density of  $\text{MnO}_2$  reaction is  $308 \text{ Wh kg}^{-1}$  for a single electron reaction [17] and the chemistry of  $\text{MnO}_2$  alkaline battery is relatively safe as it operates under aqueous media. The  $\text{MnO}_2/\text{Zn}$  alkaline chemistry has been predominantly utilised for primary batteries (non-rechargeable), however, it is receiving much attention to develop a secondary battery (rechargeable) recently [18–20].

### History

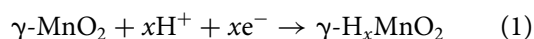
In the early stage of  $\text{MnO}_2$  electrochemistry research, the research focused on primary batteries.  $\text{MnO}_2$  was first introduced as a cathode material in a depolariser in Leclanche cell in 1866 [21]. The  $\text{MnO}_2$  cell powered early telegraphs to signal and ring an electric bell where the intermittent current was needed [22]. The first use of  $\text{MnO}_2$  in an alkaline media is developed by Leuchs in 1882 [23] where  $\text{NaOH}$  solution was used for the cell. In 1903,  $\text{KOH}$  based alkaline electrolyte was introduced by Yai [24]. Later,  $\text{KOH}$  and  $\text{NaOH}$  were used by Achenback et al. to make the first gelatinous alkaline cell [25] where they used starch to form gelatinous filling. With a powdered  $\text{Zn}$  gel anode, the revolutionary alkaline that provided enough power was developed by Urry in 1950s [26]. His alkaline battery adopted a paste electrolyte, which operated in any orientation because it has no free liquid, making it an appropriate energy source for portable equipment. Later, the demand for the alkaline  $\text{MnO}_2/\text{Zn}$  batteries increased as functional cameras and portable music players were developed in 1960–80s. In order to meet the market needs, considerable studies have been conducted to make breakthroughs by understanding the reaction mechanisms [21,27–29], enhancing performance including modifying electrode materials [17,30–35] and adjusting alkaline electrolytes [30,36,37].

Since Urry introduced a successful commercial primary  $\text{MnO}_2/\text{Zn}$  alkaline battery in the 1950s, a significant amount of work has focused on the reduction reaction mechanism of  $\text{MnO}_2$  polymorphs. In this alkaline battery section, we discuss  $\gamma\text{-MnO}_2$  or electrolytic manganese dioxide as it is the predominant polymorph adopted in commercial alkaline batteries. A number of reports found characteristic mechanisms of  $\gamma\text{-MnO}_2$  in alkaline batteries and then Chabre et al. summarised and compared the reports [21].

The mechanism proposed by Chabre is discussed in the following section.

### Reaction mechanisms

Among the polymorphs of  $\text{MnO}_2$ ,  $\gamma$ -phase is used for commercial alkaline batteries due to its ability to facilitate proton intercalation [38–40]. Numerous papers have reported reaction mechanisms of  $\gamma\text{-MnO}_2$  in the alkaline batteries, which are highly dependent on conditions including the current density, electrolyte, additive, and doping materials [21,37,41,42]. The complexity of the structural evolution of  $\gamma\text{-MnO}_2$  has been found depending on conditions, however, Chabre et al. outlined its general reaction mechanism [21]. It was demonstrated that there are two types of reactions (Figure 3) [43]: (1) a homogeneous reaction (solid-solution reaction) showing continuous voltage change and (2) a heterogeneous reaction (multi-phase reaction) with a voltage plateau. The homogeneous process is associated with the minimised lattice change and the maintained single phase of  $\gamma\text{-MnO}_2$ . Upon the reaction, the protons are introduced into the  $\text{MnO}_2$  structure.



The continuous reduction/proton insertion results in a heterogeneous reaction [27,44]. The heterogeneous process is a multi-phase transformation, which involves the co-existence of two different phases:  $\text{MnOOH}$  and  $\text{Mn}(\text{OH})_2$  [27–29].

### Bottleneck

Recently, the  $\gamma\text{-MnO}_2/\text{Zn}$  alkaline battery is revisited as a secondary battery. Ingale et al. in 2015 demonstrated that the battery is highly reversible if cycled at a reduced depth of discharge (DOD) [39]. At 10% DOD, the phase of cathode remains as pristine  $\gamma$ -

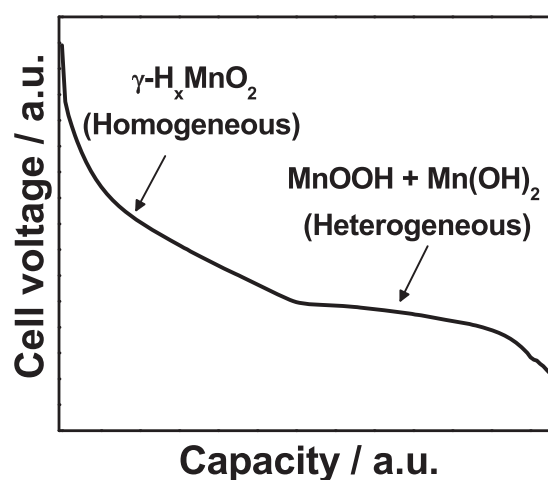


**Figure 3.** General discharge profile of  $\gamma\text{-MnO}_2$  summarised by Chabre et al. in 1995 [21].

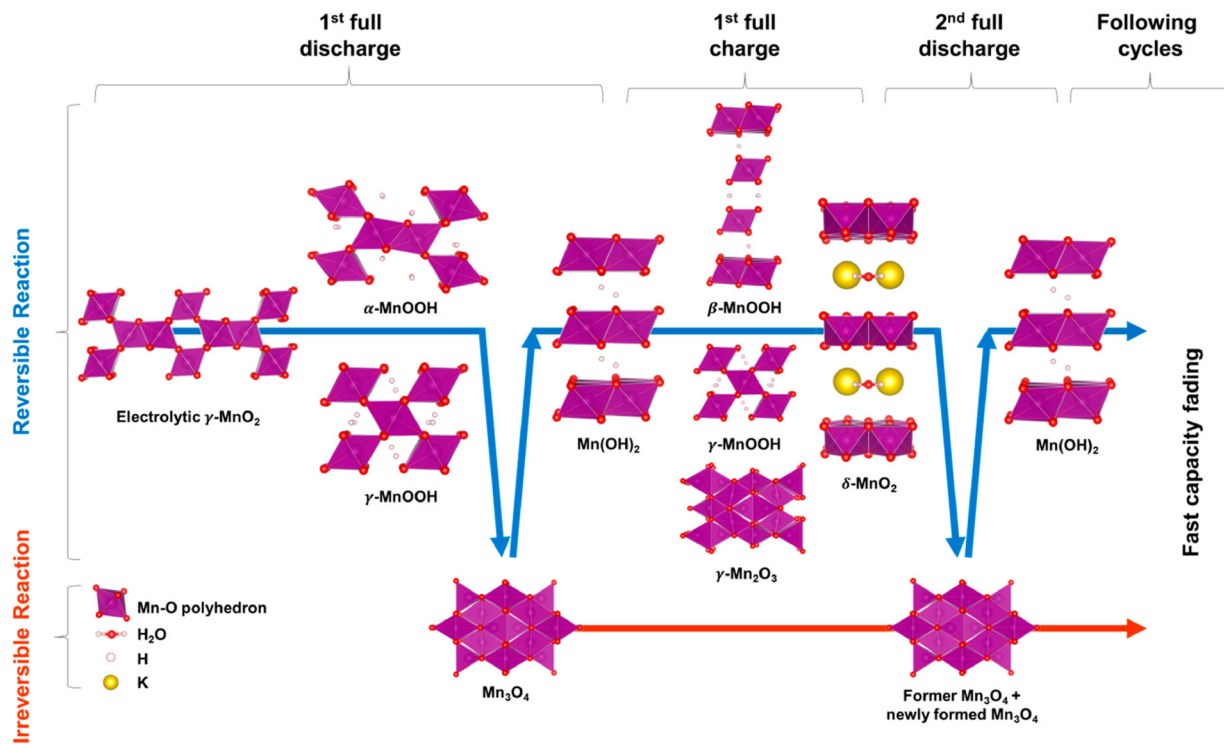


**Figure 4.** The reaction mechanism of  $\gamma$ - $\text{MnO}_2$  alkaline battery [45].

$\text{MnO}_2$ , which enables the homogeneous reaction with high reversibility. At higher DOD, however, the cathode forms irreversible phases including  $\text{Mn}_3\text{O}_4$  and  $\text{ZnMn}_2\text{O}_4$ , which limit the rechargeability of the battery. Figure 4 summarises the irreversible reaction of  $\gamma$ - $\text{MnO}_2$  in an alkaline  $\gamma$ - $\text{MnO}_2/\text{Zn}$  alkaline battery when cycled at the full DOD of theoretical two-electron reaction.

During the first discharge, the proton from an electrolyte intercalates in the  $2 \times 1$  and  $1 \times 1$  tunnels of  $\gamma$ - $\text{MnO}_2$  to form  $\alpha$ - $\text{MnOOH}$  and  $\gamma$ - $\text{MnOOH}$  phases at the end of the first electron reaction. The ratio between  $\alpha$ - $\text{MnOOH}$  and  $\gamma$ - $\text{MnOOH}$  phases is expected to be dependent on the intergrowth feature of the  $\gamma$ - $\text{MnO}_2$  structure. A bottleneck to point out is that  $\text{Mn}^{3+}$  ions in  $\text{MnOOH}$  polymorphs could undergo a disproportionation reaction, forming  $\text{Mn}^{4+}$  and  $\text{Mn}^{2+}$  species. The capacity loss could occur owing to  $\text{Mn}^{2+}$  species since it dissolves as  $\text{OH}^-$  coordinated-complex ions in a highly concentrated basic solution [46]. As the discharge goes through the second electron,  $\text{Mn}_3\text{O}_4$  [28,29] and  $\text{Mn}(\text{OH})_2$  [27,28] are generated.  $\text{Mn}_3\text{O}_4$  is a spinel structure where Mn is mixed with  $\text{Mn}^{2+}$  and  $\text{Mn}^{3+}$  oxidation states. The phase consists of tetragonal and octahedral Mn-O polyhedra.  $\text{Mn}(\text{OH})_2$ , a layered structure with a  $\text{Mn}^{2+}$  oxidation state, is created at the end of the first discharge. It is important to note that  $\text{Mn}_3\text{O}_4$  has poor electrical conductivity ( $10^8$  ohm cm), which leads to the capacity fading of the  $\gamma$ - $\text{MnO}_2$  alkaline cell [13,39]. This phase is described as a non-active phase in the electrochemical cell [28] and it only partially reduces to  $\text{Mn}(\text{OH})_2$ . This

intermediate reduction product remains in the cathode after the full discharge as well as full charge during cycles.  $\text{Mn}(\text{OH})_2$  phase, on the other hand, participates in the subsequent oxidation reaction and contributes to the partial reversibility. The cell capacity, however, decreases significantly after the first cycle because of the increased amount of  $\text{Mn}_3\text{O}_4$ .

In addition,  $\text{ZnMn}_2\text{O}_4$  or hetaerolite is another irreversible phase formed in the cathode [44,47,48]. This side product is the result of the chemical reaction between  $\text{Zn}(\text{OH})_4^{2-}$  and  $\text{MnOOH}$ . The  $\text{Zn}(\text{OH})_4^{2-}$  or Zincate ion is a redox couple with Zn anode. Once formed, it transports and reacts to the cathode where  $\text{MnOOH}$  is formed after  $\gamma$ - $\text{MnO}_2$  is reduced.  $\text{ZnMn}_2\text{O}_4$  possesses severe electrochemically inert features which show a similar resistivity with a  $\text{Mn}_3\text{O}_4$  phase [13]. In order to make a reversible two-electron  $\text{MnO}_2$  alkaline cell, it is essential to prevent  $\text{Mn}_3\text{O}_4$  and  $\text{ZnMn}_2\text{O}_4$  from forming.

## Solutions

### Electrolyte salt

Leuchs and Yai have reported the alkaline battery using different electrolyte salt [19,20]. The electrolyte salt has an effect on the electrochemical performance of  $\text{MnO}_2$  in alkaline batteries. For instance, Kozawa et al. reported the performance at various levels of KOH concentration in the electrolyte [36]. Although the higher concentration shows higher reduction capacity, it also shows more Mn dissolution, because  $\text{OH}^-$  ion binds to the  $\text{Mn}^{3+}$  to form  $\text{Mn}(\text{OH})_6^{3-}$  [13,36]. To

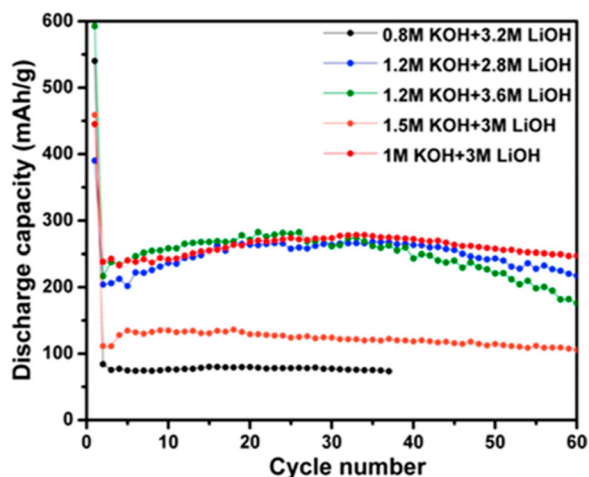


**Figure 5.** Discharge capacity of Zn/MnO<sub>2</sub> alkaline battery using the mixture LiOH and KOH electrolyte [45].

keep the stability from Mn dissolution, LiOH can be utilised in the electrolyte [37]. Unlike the KOH, utilising LiOH only exhibits less than half of the capacity, however, it promotes that Li<sup>+</sup> from LiOH intercalates in the  $\gamma$ -MnO<sub>2</sub> structure and forms the Li<sub>x</sub>MnO<sub>2</sub> spinel phase. This reaction is reversible and contributes to enhancing the cyclability. Recently, Hertzberg et al. reported that the combination of LiOH and KOH adopted in an aqueous solution of Zn/MnO<sub>2</sub> alkaline battery enhanced the rechargeability as shown in Figure 5. A reversible single-electron reaction was enabled for over 60 cycles [49]. It was proposed that a reversible reaction proceeds between reduced phases (Mn(OH)<sub>2</sub> and LiMn<sub>2</sub>O<sub>4</sub>) and oxidised phase ( $\delta$ -MnO<sub>2</sub>).

In addition, the calcium hydroxide (Ca(OH)<sub>2</sub>) sheet was reported, which improves the rechargeable reaction of a Zn/MnO<sub>2</sub> alkaline battery [50]. Instead of being used as salt in the electrolyte, the Ca(OH)<sub>2</sub> was mixed with Teflon to fabricate a sheet. The sheet is layered between a Zn anode and a separator in the battery. It is interesting to note that the concentration of zincate ion was substantially decreased during the battery's cycle when the sheet was layered. A large amount of zincate ions was confined in the Ca(OH)<sub>2</sub> interlayer and the insoluble complex calcium zincate was generated without disturbing the transport of hydroxide ions. More importantly, undesirable ZnMn<sub>2</sub>O<sub>4</sub> was not observed, which contributes to the rechargeability of the Zn/MnO<sub>2</sub> alkaline battery.

### Electrode additive

Additives are effective in improving cycling performance; for example, alkaline earth oxides such as MgO and BaO [17]. The oxides could be physically mixed with the  $\gamma$ -MnO<sub>2</sub> cathode. Compared with the pristine  $\gamma$ -MnO<sub>2</sub> cathode, BaO added  $\gamma$ -MnO<sub>2</sub> cathode shows improved cycle performance, however, its capacity over prolonged cycles decays due to the formation of

irreversible ZnMn<sub>2</sub>O<sub>4</sub> phase. Adding MgO demonstrates more stable cycling capacity than adding BaO and hinders the ZnMn<sub>2</sub>O<sub>4</sub> formation. The combination of MgO and BaO may help in gaining a high retention capacity and alleviating the formation of ZnMn<sub>2</sub>O<sub>4</sub>. Furthermore, Ba(OH)<sub>2</sub> has shown to inhibit the Mn<sup>3+</sup> dissolution and suppresses undesirable  $\delta$ -MnO<sub>2</sub> and Mn<sub>2</sub>O<sub>4</sub> formations [51]. Ba(OH)<sub>2</sub> additive significantly decreases the charge-transfer resistance of the  $\gamma$ -MnO<sub>2</sub> electrode [34]. It is suggested that Mg and Ba compounds generate ZnO-Mn<sub>2</sub>O<sub>3</sub>. When Zn<sup>2+</sup> ions migrate from the anode to the cathode side, it reacts with the MnO<sub>2</sub> to form a resistive and irreversible ZnMn<sub>2</sub>O<sub>4</sub> phase. The Mg and Ba compounds alleviate the formation of this ZnMn<sub>2</sub>O<sub>4</sub> phase.

Similarly, Bi<sub>2</sub>O<sub>3</sub> additive is widely utilised as a MnO<sub>2</sub> additive due to its ability to improve cycle retention. The Bi<sub>2</sub>O<sub>3</sub> improves the retention by suppressing the unwanted birnessite ( $\delta$ -MnO<sub>2</sub>) and hausmannite (Mn<sub>3</sub>O<sub>4</sub>) phases from forming [52–54]. Additional reports utilising BaBi<sub>2</sub>O<sub>3</sub> [52], NaBiO<sub>3</sub> [53], Ag<sub>4</sub>Bi<sub>2</sub>O<sub>5</sub> [55], and Bi<sub>2</sub>O<sub>3</sub>-Cu [56] additives further proves the effectiveness of the Bi<sub>2</sub>O<sub>3</sub>. Minakshi and Mitchell in 2008 suggested that the Bi<sup>3+</sup> permits a deeper DOD by reducing the magnitude of structural changes in  $\gamma$ -MnO<sub>2</sub> cathode during cycling [57]. The exact reason for causing such a favourable phase transformation in the  $\gamma$ -MnO<sub>2</sub> cathode is still unclear. The Bi<sub>2</sub>O<sub>3</sub> additive is also known to improve the Zn anode cycle retention by forming more planar and less dissolvable Zn [48,58]. Preventing the Zn<sup>2+</sup> ions from reacting with the cathode may also allow deeper DOD and formation of more favourable phase formations.

There are several additives that affect the phase transformation of the  $\gamma$ -MnO<sub>2</sub> reacting with H<sup>+</sup> ion. On the other hand, additives such as TiB<sub>2</sub> and B<sub>4</sub>C suppress the  $\gamma$ -MnO<sub>2</sub> reaction with H<sup>+</sup> ion. Minakshi et al. in 2010, demonstrated Zn/MnO<sub>2</sub> alkaline battery with LiOH electrolyte [59,60]. A small amount of B<sub>4</sub>C was added to the cathode to observe improved first cycle discharge capacity but lowered reaction voltage. They claim that the 'boron broadens the pathway between the structural chains of MnO<sub>6</sub> octahedra for the diffusion of lithium in the MnO<sub>2</sub> host and stabilise the structure [60].' They have also shown that in KOH electrolyte, the K<sup>+</sup> ions do not effectively diffuse in the MnO<sub>2</sub> host. The B<sub>4</sub>C additive promotes Li<sup>+</sup> ion insertion reaction but not H<sup>+</sup> nor K<sup>+</sup> ion insertion. Similarly, TiB<sub>2</sub> additive has also demonstrated to be able to promote Li<sup>+</sup> ion insertion in the LiOH electrolyte [30,61]. Due to the Li<sup>+</sup> ion insertion reaction, Minakshi et al. in 2008, has shown that the initial discharge capacity increases from 150 mAh g<sup>-1</sup> to 220 mAh g<sup>-1</sup>, but with considerably worse rechargeability [61]. The interesting feature here is that in KOH electrolyte, TiB<sub>2</sub> promotes K<sup>+</sup> ion insertion as well [30]. These boron containing cathode additives are effective in

increasing the initial discharge capacity by promoting alkali metal cation diffusions. However, these additives lack the ability to improve the cycle retention. On the other hand, with the addition of another additive, such as  $\text{Bi}_2\text{O}_3$  to stabilise the  $\text{MnO}_2$  phase transformation, the cycle retention can be optimised [30,62,63].

### pH of the electrolyte

Under the high concentration of hydroxide ion at  $\text{pH} > 7$ , the Zn anode has a redox couple with the zincate ion, which eventually generates the irreversible  $\text{ZnMn}_2\text{O}_4$  phase regardless of adopting any materials in the alkaline battery to prevent its formation. In the past few years, several studies have reported high performed Zn/ $\alpha$ - $\text{MnO}_2$  aqueous batteries in weak acidic electrolytes [19,64,65]. Lee et al. demonstrated that a Zn/ $\alpha$ - $\text{MnO}_2$  aqueous cell in  $\text{ZnSO}_4$  electrolyte undergoes  $\text{Zn}/\text{Zn}^{2+}$  and  $\alpha$ - $\text{MnO}_2/\text{Mn}^{2+}$  reaction at the anode and the cathode, which are reversible [65]. Another reversible reaction contributes to the enhanced cyclability;  $\text{Zn}_4(\text{OH})_6(\text{SO}_4) \cdot 5\text{H}_2\text{O}$  (zinc hydroxide sulphate) was found to precipitate on the surface of cathode due to  $\text{Zn}^{2+}$  and  $\text{SO}_4^{2-}$  in aqueous electrolyte. In addition, Pan et al. described that  $\text{MnSO}_4$  salt in the  $\text{ZnSO}_4$  electrolyte significantly improves the rechargeability of Zn/ $\alpha$ - $\text{MnO}_2$  aqueous battery [19]. The same redox reactions in cathode/anode proposed by Lee et al. [65] was characterised by an undefined hydration number for the zinc hydroxide sulphate. The significant difference is analysed, however; adding  $\text{MnSO}_4$  salt in the electrolyte

alleviates  $\text{Mn}^{2+}$  dissolution, which allows the life span of over 5000 cycles. Also, Pan et al. described that the stability and reversibility of Zn in the weak acidic electrolyte is improved compared with Zn in the base electrolyte in Figure 6. Their Zn/Zn symmetric cell in the weak acidic solution exhibited a smooth and dense Zn surface during cycles, however, the one in the base solution displayed a loose and powder-like Zn surface due to the formation of irreversible phase.

### Morphology

Rechargeable alkaline battery undergoes not only conversion reactions but also intercalation reactions [54,66,67]. To be able to access deep DOD, it is important to utilise both the reactions. However, unlike the highly reversible intercalation reaction, the conversion reaction is prone to forming unwanted phases those lead to low cycle retention. Therefore, to improve the cycle retention, synthesising a  $\text{MnO}_2$  that promotes intercalation reaction can be a good solution. Tompssett et al. reported that the direction perpendicular to (001) surface in  $\beta$ - $\text{MnO}_2$  shows small Li diffusion barrier compared to (010) and (111) surfaces [68]. [001] direction possess low migration barrier owing to less distortion of the  $\text{MnO}_6$  polyhedron along that direction. Exposing a large area of (001) surface on  $\beta$ - $\text{MnO}_2$  facilitates cation intercalations since the surface possess metallic states promoted by spin-polarised surface oxygen [69]. Synthesising (001) surface-oriented  $\beta$ - $\text{MnO}_2$  morphology can facilitate the intercalation reaction and improve the cycle retention.

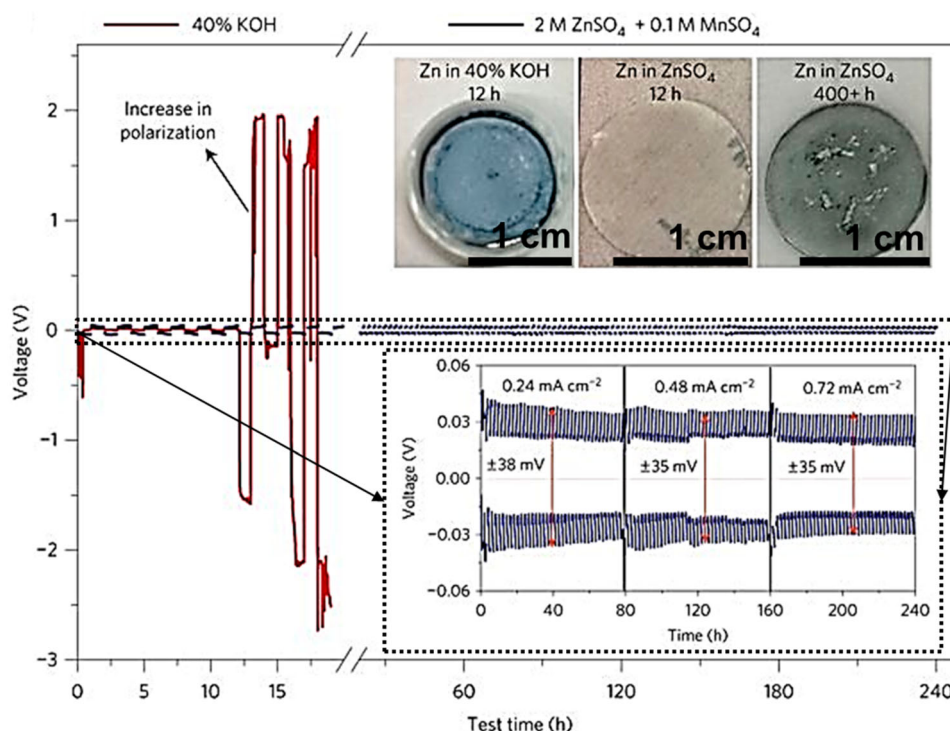


**Figure 6.** Zn stripping/plating from Zn/Zn symmetrical cells in the 40% alkaline electrolyte and in the 2 M  $\text{ZnSO}_4$  with 0.1 M  $\text{MnSO}_4$  weak-acid electrolyte, respectively. The inset images are cycled Zn anodes in alkaline and weak-acid electrolytes [19].

In addition to the importance of surface-oriented morphology, nanoscale  $\text{MnO}_2$  synthesis is another factor affecting the performance of alkaline batteries. Cheng et al. demonstrated that 1-D nano-structured  $\alpha$ - and  $\gamma$ - $\text{MnO}_2$  exhibit favourable electrochemical performance in alkaline batteries [70]. Large surface area to volume ratio in nano  $\text{MnO}_2$  provides more active sites compared to the bulk  $\text{MnO}_2$  resulting in better electrode performance. Zhang et al. summarised synthesis methodologies for various nano morphologies and concluded that high surface area of nanoscale  $\text{MnO}_2$  ameliorates contact between  $\text{MnO}_2$  surface and the electrolyte leading to low internal resistance, fast cation diffusivity, and high utilisation efficiency [71].

### Outlook

The rechargeable  $\gamma$ - $\text{MnO}_2/\text{Zn}$  alkaline battery with high DOD is one of the promising large-scale EESS in the near future, yet this battery still needs to be refined for the commercial market. The one-electron reaction is higher in voltage than the two-electron reaction. If the DOD of the one-electron reaction can be improved, the capacity of the alkaline battery would dramatically increase. Aside from the additives, simply optimising the DOD can also elevate the capacity and cycle retention. In addition, it is evident that the use of  $\text{LiOH}$ ,  $\text{KOH}$ , and  $\text{Ca}(\text{OH})_2$  predominates the field. While these types of salt have a great influence on the battery mechanism, another electrolyte salt also can be proposed. More characterisation and mechanistic studies of possible salt in the alkaline battery are necessary. In the case of additives, mechanistic studies conducted on the oxide additives show possibilities in stabilising the cycling capacity. Such a mechanism has guided to mix different metal oxides together. The two additives serve a different and complementary purpose and together, boosting the cycle performance. The control of pH could be also considered to improve the reversible reaction in cathode/anode. The characterisations of the unwanted and wanted phases have been conducted only recently. Further understanding of the structural evolution to propose plausible ways to make breakthroughs is needed.

### Supercapacitor

#### $\text{MnO}_2$ in supercapacitor

The EESS technology, especially LIBs, has been greatly developed over the past decade to solve the issues of intermittent power generations [1,72]. LIBs dominate the EESS market as they currently offer the best combination in terms of specific energy, power, cost, and device lifetime [73–76]. Nevertheless, there is significant attention drawn to EESS devices that can charge

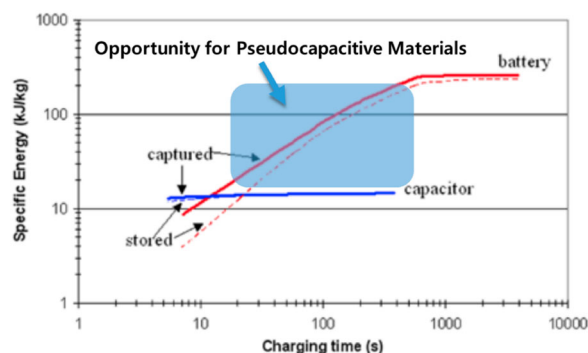


**Figure 7.** The region where supercapacitors outperform batteries, about 10 s [77].

in a second-to-minute regime rather than an hour regime (Figure 7). The second-to-minute regime is where supercapacitors thrive, although such devices are currently impeded from larger market adoption due to low energy density [78–80]. As such, much research in the past 15 years has been focused on improving the energy density of supercapacitors; the bulk of these endeavours have been directed towards pseudocapacitive materials such as  $\text{RuO}_2$  or  $\text{MnO}_2$  [81,82]. The pseudocapacitors are supercapacitors, which undergo both surface and bulk reactions. Consequently, the energy density of pseudocapacitors is remarkably higher in the category of capacitor technologies [83,84–86].  $\text{RuO}_2$  possesses high theoretical capacitance of approximately  $1450 \text{ F g}^{-1}$  and electronic conductivity of  $10^4 \text{ S cm}^{-1}$  [87,88]. However,  $\text{RuO}_2$  suffers from being extremely expensive, not earth-abundant, and somewhat toxic [77].  $\text{MnO}_2$ , on the other hand, also has a high theoretical capacitance of  $1250 \text{ F g}^{-1}$ , yet the conductivity of  $\text{MnO}_2$  is much lower; ranging from  $10^{-7}$ – $10^{-3} \text{ S cm}^{-1}$  [89–91]. Another benefit of  $\text{MnO}_2$  is cheap material cost, plentiful in the earth's crust, and environmentally benign. It is clear that advances in a pseudocapacitor technology should be made to take advantage of those benefits towards the large-scale applications.

### History and mechanism

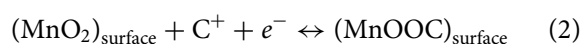
Present-day supercapacitor technology relies heavily on the electric-double-layer capacitance (EDLC) mechanism. The first obtained patent in 1957, the charge storage in an EDLC device is explained by the Helmholtz model [92–95]. At the discharged state of the cell, the net charge on the electrode surface is created. Cations ( $\text{K}^+$ ,  $\text{Na}^+$ ,  $\text{Li}^+$ , etc.) and anions ( $\text{SO}_4^{2-}$ ,  $\text{OH}^-$ , etc.) are surrounding each other in aqueous electrolyte and are randomly arranged. At the discharged state, cations are electrostatically attracted to the anode surface and so are the anions to the cathode surface. The resultant layers of charge are separated everywhere from a monolayer to a few molecules-thick layers of

solvent molecules. This near-molecular dielectric layer provides a small charge separation distance and results in a high capacitance ( $C$ ), governed by  $C = (\epsilon A/d)$ , where  $A$  is the area of the electrode,  $\epsilon$  is the permittivity in vacuum, and  $d$  is the dielectric layer thickness [92]. EDLC utilises little to none faradaic reactions between the electrode and the electrolyte. EDLC yields fast kinetics and little disruption of the electrode structure, resulting in high power but limited in the energy [89–91,94]. Charge storage is largely determined by the surface area, thus activated carbon electrodes with the high surface area are commonplace [89–91,94]. However, it is shown that enlarged surface area does not necessarily translate into elevated capacitance, because pore sizes and surface defects also play an important role [96]. Regardless, the lack of bulk charge storage in EDLC electrode material limits specific capacitance up to  $200 \text{ F g}^{-1}$  [89–91,94].

A pseudocapacitive material undergoes fast faradaic reactions to store charge on and beyond the electrode surface. A pseudocapacitive material has the characteristic electrochemical behaviour: a linear increase or decrease of voltage with respect to charge or discharge of capacitance (Figure 8) [98]. The ideal supercapacitor has rectangular cyclic voltammetry (CV) behaviour governed by the EDLC [77,97,99–101]. The CV of the ideal pseudocapacitor also acts in a rectangular manner while the rectangle is originated not only from the EDLC but also from the capacitance beyond the surface. The battery has asymmetric faradaic

peaks with minimum rectangular behaviour [77,97,99–101]. Thus, pseudocapacitor operates under charge storage mechanisms similar to that of the battery materials and the thermodynamic relation between charge and voltage gives rise to a capacitive behaviour. There is only a subtle difference between the battery and pseudocapacitor materials. For instance,  $\text{LiCoO}_2$ , a common LIB cathode material exhibits a pseudocapacitance behaviour when it is nano-sized (Figure 8(d)) [77,97]. Additional CV analysis at various sweep rates can be taken to fit the data to an equation:  $i = av^b$  where  $i$  is current,  $v$  is voltage sweep rate, and  $a$  and  $b$  are constants. For a battery material,  $b = 0.5$  and for a pseudocapacitive material  $b = 1.0$  [77,97].

$\text{MnO}_2$  is a pseudocapacitive material. The advantage of these materials is that charge can be stored on the surface and in the bulk of the material [87,102–104]. The reactions are as follow:



where  $\text{C}^+ = \text{Na}^+, \text{Li}^+, \text{K}^+$ , etc. The pseudocapacitors such as  $\text{MnO}_2$ s utilise both the surface EDLC and bulk intercalation. They result in higher specific capacitance than solely EDLC-based supercapacitors [89–91,94]. However, the bulk storage kinetic is slower than the EDLC charge storage mechanism because of the slow diffusion of cations. The power is stronger than that of batteries and the energy density is greater than EDLC-based supercapacitors. There is a trade-off in switching to pseudocapacitive materials; much higher energy density is achieved at the expense of power. Therefore, pseudocapacitors enable a second-to-minute scale load levelling on the electrical grid. A supercapacitor refers to a device or material exhibiting pseudocapacitive characteristics for the remainder of this review.

### Bottleneck

Although  $\text{MnO}_2$  is an ideal material, it has three main problems: (1) low electronic conductivity, (2) dissolution of Mn into the electrolyte, and (3) unstable volume expansion [89–91]. First,  $\text{MnO}_2$  has very low electronic conductivity [89–91]. As a result, the diffusion of ions throughout the material is slow and drastically reduces the power density. The sluggish diffusion brings out poor ion percolation across the electrodes and inhibits the amount of energy that can be stored in a bulk electrode [89–91]. Toupin et al. demonstrated that the bulk charge storage only takes place in a thin layer on the surface of the electrode [102]. This causes thick composite electrodes to fall short of the theoretical capacity of  $1250 \text{ F g}^{-1}$ , achieving merely about  $200 \text{ F g}^{-1}$  [104,105]. Such property

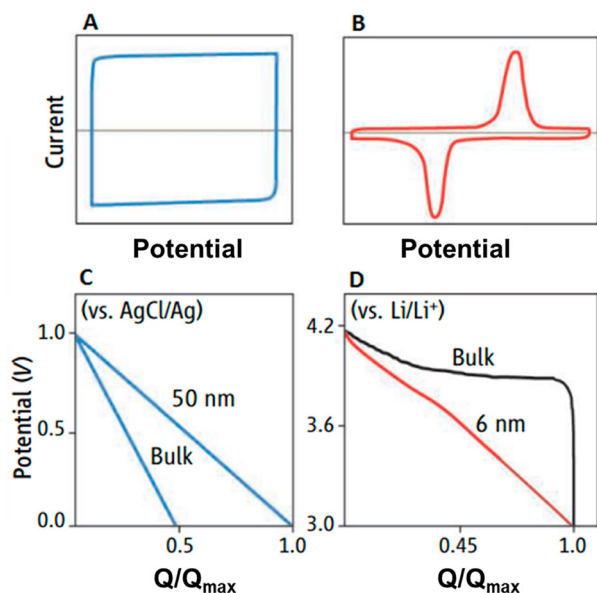


**Figure 8.** (a) Shows the rectangular cyclic voltammogram of an intrinsic pseudocapacitor compared to (b) the asymmetric redox peaks of battery material. (c) Illustrates the constant voltage profile of a true pseudocapacitive material in both bulk and nanosized regimes. (d) Displays that nanoscale battery material exhibits a sloping voltage profile in contrast to the constant voltage of bulk battery material, giving a prime example of an extrinsic pseudocapacitive material behaving as an intrinsic pseudocapacitor [97].

is one of the main reasons for utilising the supercapacitor as a load leveller in the high-frequency region not the main energy storage device. Much of the research on MnO<sub>2</sub> has focused on enhancing the power density through increasing conductivity and surface area. The second hurdle of utilising MnO<sub>2</sub> is that manganese slowly dissolves into the electrolyte *via* a disproportionation reaction [83,84,106]:



The capacity of the electrode decreases at a steady rate as Mn<sup>2+</sup> enters the electrolyte, subsequently lowering the lifetime of the pseudocapacitor device. Lastly, MnO<sub>2</sub> structures experience volume expansion of varying degrees, which causes the loss of electrical contacts between MnO<sub>2</sub> particles, increasing resistivity, and lowering capacitance over time [85,86,107,108]. These issues have a direct negative effect on the power density and cycle life of pseudocapacitors.

## Solutions

### Nano particles

One way to boost the power density is nanostructuring the particle and expanding the surface area. Nanostructuring MnO<sub>2</sub> electrodes to create a wider specific surface area is a promising method of enhancing two aspects of MnO<sub>2</sub>: First, the enlarged surface area produces a broader electrolyte/electrode interface, which increases surface charge storage. Second, because nanostructures have short diffusion pathways, nanostructuring can largely obviate the inherently low conductivity of MnO<sub>2</sub>. For example, 2 nm × 8 nm sized α-MnO<sub>2</sub> nanoneedle (400 F g<sup>-1</sup>) has higher capacitance compared to 10 nm × 100 nm sized α-MnO<sub>2</sub> nanoneedle (297 F g<sup>-1</sup>) [109,110]. Besides making the nanoparticle MnO<sub>2</sub>, a common method to improve the electric conductivity of the electrode is by simply mixing in some conductive carbon [111]. Although adding conductive carbon allows the electron to be evenly distributed throughout the whole composite electrode, there are tradeoffs: the active mass loading decreases and the conductive carbon covers the active surface. Furthermore, increasing the composition of low-density materials such as conductive carbon leads the electrode to be thicker. The thick electrodes force the electrons to travel farther distance. In a way, the addition of conductive carbon works against the power density because the electrons have to travel farther distance. There is an optimum amount of the carbon between increasing electrical conductivity and covering too much of the active surface [110].

### Nano electrodes

It is noted that the nanoparticle enhances the supercapacitor performance, however, for the smaller particles,

more conductive carbon needs to be utilised to electrochemically link wider surface area. Further research has focused on fabricating free-standing MnO<sub>2</sub> on the conductive substrate instead of fabricating the composite electrode with the powder MnO<sub>2</sub>. A nanowire of MnO<sub>2</sub> was deposited on a smooth conductive substrate and the capacitance has increased to >400 F g<sup>-1</sup> [112]. However, with the smooth substrate, the areal active mass loading is low compared to that of the composite electrodes, which leads to smaller areal energy density. Yet, the free-standing MnO<sub>2</sub> electrodes are consistently superior to the composite electrodes in terms of the gravimetric energy density [88,112–122].

Porous substrates can be utilised to broaden the areal substrate surface instead of the smooth substrate to fabricate the free-standing MnO<sub>2</sub> (Figure 9) [123]. The areal loading of the MnO<sub>2</sub> is drastically increased. When MnO<sub>2</sub> is deposited on a 350 μm-thick film of multi-walled carbon nanotubes *via* Lu et al.'s method, gravimetric capacity exceeds 1250 F g<sup>-1</sup> [124]. Although the active mass loading is not reported, significantly higher mass loading is anticipated than that of the single flat substrate. This work deposited MnO<sub>2</sub> at 70 nm in thickness and achieved the theoretical capacitance of MnO<sub>2</sub> [124]. There are multiple similar reports utilising thin MnO<sub>2</sub> deposition to obtain both high capacitance values and full energy density [125–127]. The thin deposition of MnO<sub>2</sub> on porous substrates to increase the areal loading is a good strategy to increase the energy density without compromising the power density. However, it is important to keep in mind the manufacturing cost. The material cost is low due to utilising MnO<sub>2</sub> but if the cost of substrate increases, the MnO<sub>2</sub> supercapacitor system may not be cost effective.

### Doping

While the physical alterations *via* nanosizing and deposition methods are effective, doping alters the intrinsic chemistry of the MnO<sub>2</sub>. Computational methods are extremely valuable in proposing a potential material. For instance, Au ion can be doped into MnO<sub>2</sub> [128]. Computationally, the presence of Au ion near the Mn ions bridges the band gap and enhances the conductivity. Experimentally, the capacitance increases by 65%, however, utilising Au as a dopant may work against the use of low-cost Mn. Although more work is needed, it can be assumed that a similar effect can be expected with Cu and Ag ion in the place of Au ion [129]. Recently, Liu et al. doped δ-MnO<sub>2</sub> with cost-effective vanadium [130]. The V<sup>5+</sup> ions substituted K<sup>+</sup> ions in the interlayer position and Mn<sup>4+</sup> ions were placed in the MnO<sub>6</sub> octahedral layer. As a result, the interlayer distance is shortened while lowering the charge transfer resistance.

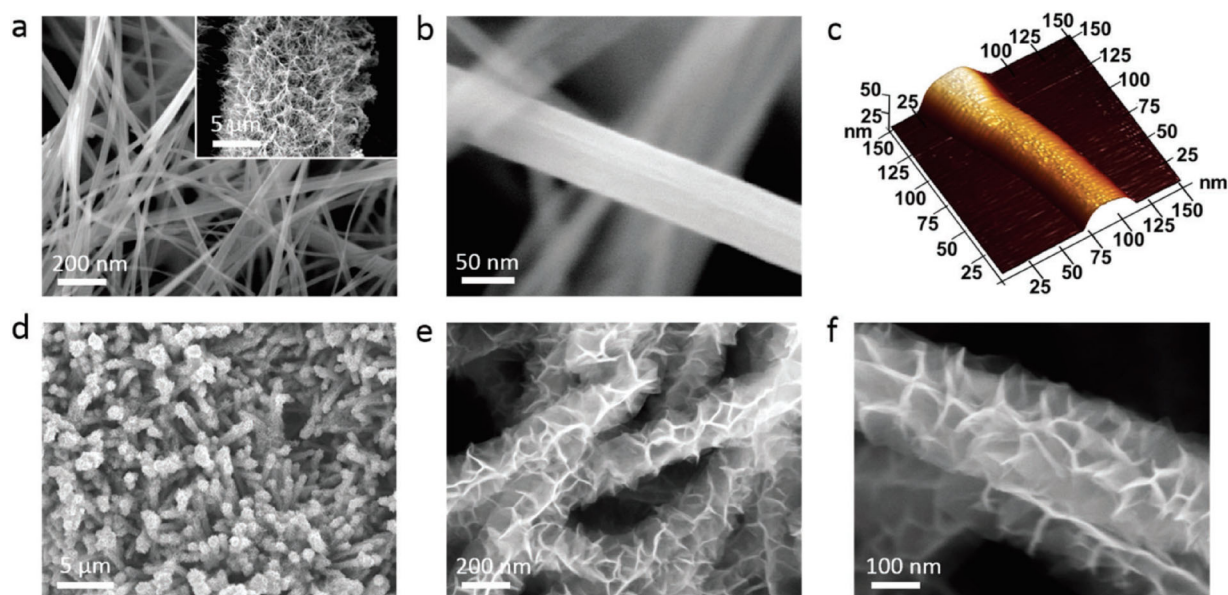


**Figure 9.** Images of (a and b) nanowire  $\text{MnO}_2$ . Inset of a is the nanowire under low magnification showing the homogeneous distribution of the wires on a carbon fibre. (c) AFM 3D image of a single nanowire. (d and e). The as-synthesised free-standing  $\text{MnO}_2$  electrode and (f) after annealing [123].

### Phase distinction

Although much of the research on supercapacitor has focused on nanostructuring, it is notable that polymorphs of  $\text{MnO}_2$  store different amounts of capacitance. Ghodbane et al. conducted a study on the performance of various  $\text{MnO}_2$  polymorphs, including 1-D tunnel structures, 2-D layered structures, and 3-D spinel structures (Figure 10) [131]. The general trend is that conductivity, surface area, and specific capacitance increase as network dimensions expands [131]. More specifically, the cryptomelane structure has a smaller surface area than that of the Ni-todorokite structure, yet its capacitance is higher. This arises from cations utilised in the synthesis or other molecules blocking ionic conduction pathways. The crystal

structure, which affects the accessibility of the electrolyte, has more influence on the capacitance than the surface area. The surface area data for exceptionally porous materials must be taken cautiously because the adsorbent gas used in measurement may not access all regions. The work by Brousse shows that the wider the surface area is, the larger the capacitance becomes [132]. However, Brousse's work also includes the low capacitance/high surface area outliers, highlighting the need for investigating beyond the surface area and considering polymorphs. A wide array of polymorphs and morphologies are found in the literature and their disparate range of performances requires careful consideration of the polymorphs used in experimentation.

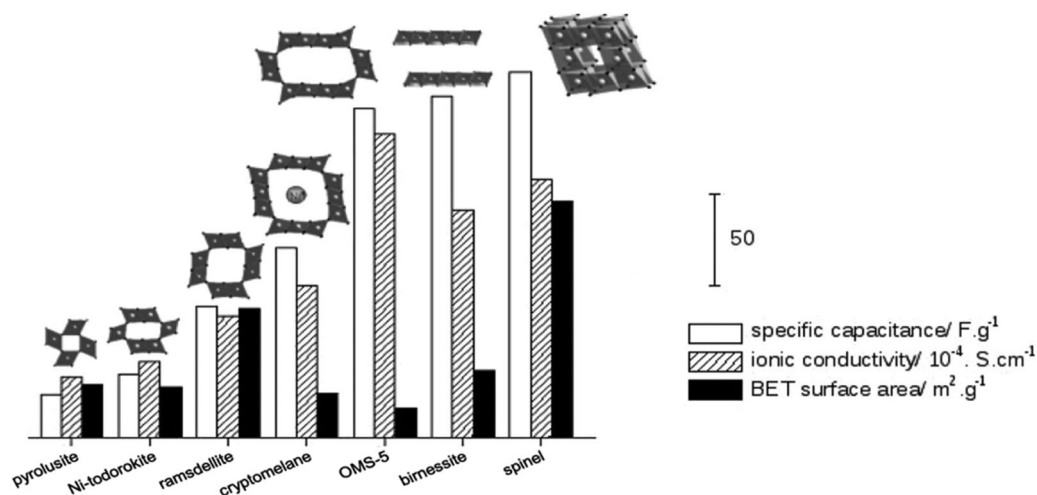


**Figure 10.** Compares specific capacitance, ionic conductivity, and Brunauer-Emmett-Teller surface areas of various  $\text{MnO}_2$  polymorphs with varying dimensions of conductivity (left to right is 1-D to 3-D) [131].

### Electrolyte

Lastly, the pseudo-capacitive reactions are governed by the surface and bulk intercalation reaction between the cation of the electrolyte and the  $\text{MnO}_2$  active material. There are numerous reports on various cation ( $\text{Li}^+$ ,  $\text{Na}^+$ ,  $\text{K}^+$ ,  $\text{Ba}^{2+}$ ,  $\text{Mg}^{2+}$ , and  $\text{Ca}^{2+}$ ) insertions into the  $\text{MnO}_2$  lattice [133–138]. These cations vary in their ionic radius, which affects the diffusion of cations from the surface to the bulk of the  $\text{MnO}_2$ . For instance, with the  $\delta$ - $\text{MnO}_2$ , 0.5 M  $\text{Na}_2\text{SO}_4$  electrolyte exhibits higher capacitance than 0.5 M  $\text{Li}_2\text{SO}_4$  at 30  $\text{mV s}^{-1}$  rate. At a slower rate, the  $\text{Li}_2\text{SO}_4$  electrolyte shows higher capacitance [138]. In addition to the ionic radius, unlike the monovalent alkaline metal ions, the alkaline-earth metal ions are divalent. The ionic radius is similar to that of the monovalent  $\text{Li}^+$  ion and  $\text{Mg}^{2+}$  ion has a twofold charge. The divalent electrolyte with ion consistently has the superior capacitance to the monovalent electrolyte with ion [134,138]. However, when the divalent cation diffuses into  $\text{MnO}_2$  and reduces the  $\text{Mn}^{4+}$  into  $\text{Mn}^{2+}$ , the  $\text{Mn}^{2+}$  ion is prone to dissociate. Because forming  $\text{Mn}^{2+}$  diminishes capacitance in prolonged cycles, all  $\alpha$ -,  $\gamma$ -, and  $\delta$ - $\text{MnO}_2$  have more stable electrochemical cycles in 0.5 M  $\text{Li}_2\text{SO}_4$  electrolyte than in 1.0 M  $\text{Mg}(\text{NO}_3)_2$  electrolyte [138].

### Outlook

Since the specific capacitance over 1000  $\text{F g}^{-1}$  is achievable with an energy density of 49–135  $\text{Wh kg}^{-1}$  and power density of 1.0–17.4  $\text{kW kg}^{-1}$  [124], further effort needs to focus on the often-neglected shelf-life and self-discharge. Although it is often ignored in the  $\text{MnO}_2$  supercapacitor research, a shelf-life is a vital performance parameter [139]. Research on the shelf-life of EDLC capacitors exhibits that 5–15% of capacity is lost after 48 h on standby and over 20% after 200 h [140,141]. Barely any extensive research has been done on the self-discharge of  $\text{MnO}_2$  supercapacitors. Among some mechanisms for self-discharge, a popular mechanism is the charge redistribution and activation-controlled self-discharge [142]. Much more research is needed to understand the self-discharge in  $\text{MnO}_2$  supercapacitors and self-discharge properties need to be discussed with other properties such as specific capacitance.

Various nanoparticles of  $\text{MnO}_2$  are reported in the literature, yet  $\text{MnO}_2$  nanoparticles incorporated into binder/carbon black composites with high loading provide little benefit. This is due to the necessity of excessive addition of carbon and/or binder, which brings down the active mass loading. These additives block the active surface area of the  $\text{MnO}_2$ . Numerous forms of  $\text{MnO}_2$  electrodes exist and thin-film  $\text{MnO}_2$  deposition onto a high surface area substrate offers the highest capacitance. Doping methods are also promising that they facilitate the possibility to intrinsically

eliminate the disadvantages. The conductivity is enhanced by altering the electronic structure of  $\text{MnO}_2$  allowing higher loading and more commercial applicability. The nature of doping or coating's positive effect still remains unclear, thus more parameters such as crystal structure, surface area, loading, and electronic structure are to be observed and reported.

### Lithium-ion battery

#### $\text{MnO}_2$ in LIB

Aside from alkaline batteries, LIBs predominantly employ reversible intercalation of  $\text{Li}^+$  in and out of the host structure. They have become the alternative energy supply for portable devices [143]. They have excellent energy density and cyclability because of the electrode materials hosting  $\text{Li}^+$  without a significant change of its crystal structure [143]. Despite the excellent advantages in performance, it still suffers from its high fabrication cost and safety. A commonly known LIB system makes use of organic electrolytes that are stable in a wide voltage window. Beck and Ruetschi highlighted the 'Three E' criteria; energy, economics, and environment to determine the suitable energy storage system [144]. Utilising the organic electrolyte allows the batteries to produce high power and energy due to its high voltage, however, the organic electrolytes are expensive because they require high purity and are sensitive to moisture. Such electrolytes are highly flammable which raise safety concerns. Replacing the organic electrolyte with aqueous electrolyte can drastically reduce the cost of the battery and eliminate the safety concern from flammability. This section focuses on the progress of the aqueous rechargeable LIB.

A spinel phase,  $\text{LiMn}_2\text{O}_4$ , intercalates  $\text{Li}^+$  ion. As mentioned above, the mechanism involves  $\text{Li}^+$  ion intercalation in the interstitial sites of the host material. Since using aqueous electrolyte, the possibility of proton intercalation needs to be discussed. The intercalation of proton often results in degrading cycling capacity. When the protons are generated as a result of electrolyte oxidation, it can replace the electrochemically extracted  $\text{Li}^+$  in the structure [145]. The capacity decays because the interstitial sites for  $\text{Li}^+$  are occupied by the proton and it hinders  $\text{Li}^+$  intercalation. Besides the presence of protons in the site for  $\text{Li}^+$  insertion, it creates sheer stress between the oxygen layers due to strong O–H–O bonding. Eventually, the protons alter their crystal structure [146]. Thus the proton insertion makes the structural changes associated with the poorly electroactive hausmannite  $\text{Mn}_3\text{O}_4$  phase [147]. The crystal structure has a major role in the selectivity towards proton intercalation. It is notable that not all structures allow such intercalations; the proton

insertion is less favourable in both spinel and olivine structures compared to the layered structures [148].

### History and mechanism

The concept of LIB involving the  $\text{Li}^+$  ion intercalation is introduced by Dahn et al. in 1994 [149]. The  $\text{Li}^+$  ion intercalation is the diffusion of  $\text{Li}^+$  ions in and out of the interstitial sites of the electrode material. When the  $\text{Li}^+$  ion is inserted into the host structure, the oxidation state of the host changes, but the crystal structure change is minimum because the  $\text{Li}^+$  ion is relatively small. This results in good cycling retention. As mentioned earlier, there are three major types of cathode materials for LIB: layered, spinel, and olivine. The spinel structure, especially the  $\text{LiMn}_2\text{O}_4$  benefits from the abundance, low cost, and environmental friendliness of Mn.  $\text{Li}^+$  ions occupy tetrahedral 8a sites and  $\text{Mn}^{3+/4+}$  ions occupy octahedral 16d sites in a cubic close-pack array of oxygen anions (Figure 11). During the intercalation,  $\text{Li}^+$  ion diffuses through vacant tetrahedral and octahedral interstitial sites in the 3-D structure. With the spinel  $\text{LiMn}_2\text{O}_4$ , Li can be etched out of the spinel structure using acid without destructing the spinel structure, known as  $\lambda\text{-MnO}_2$  [150]. Since the discovery of LIB system, a number of papers have been published (Figure 2(a)), yet the amount of research on the aqueous rechargeable LIB was limited due to its lower power density than the organic LIB until 2006. The rising concern for the safety and cost of the organic electrolyte has driven researchers to conduct more research on the aqueous electrolyte. Initially, it was considered that the aqueous LIB has poor cycling performance, however, after more than a decade of research and development, the performance has greatly improved with longer cyclability and higher rate capability [151].

### Bottleneck

The spinel  $\text{LiMn}_2\text{O}_4$  structure is an insulating material [149]. Due to its lack of electrical conductivity, the conductive additive or other forms of treatment are required for the spinel  $\text{LiMn}_2\text{O}_4$  to function as an electrode material. At its pristine state, there is an equal amount of  $\text{Mn}^{3+}$  and  $\text{Mn}^{4+}$ . Depending on the

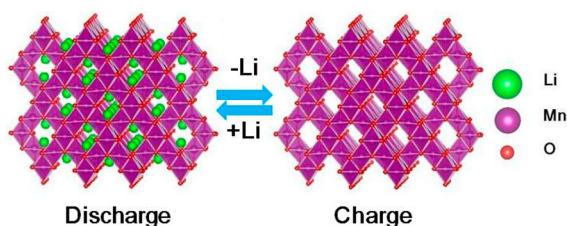


**Figure 11.** Crystal structure of  $\text{LiMn}_2\text{O}_4$  (left) and  $\lambda\text{-MnO}_2$  (right) after Li has been either etched or diffused out.

direction of the  $\text{Li}^+$  intercalation,  $\text{Mn}^{3+}$  can oxidise to  $\text{Mn}^{4+}$  or  $\text{Mn}^{4+}$  can reduce to  $\text{Mn}^{3+}$  [152]. Unfortunately, utilising Mn-based redox in a LIB has a major intrinsic disadvantage. While the advantage of  $\text{LiMn}_2\text{O}_4$  is the minimum structural deformation, the disadvantage is the use of Mn redox.  $\text{Mn}^{3+}$  has Jahn–Teller distortion [153] which largely changes the bond length between the axial and equatorial Mn–O bond of the Mn octahedral coordination. This change can introduce a strain that derives local plastic deformation and 5.6% of volume distortion [85,86]. Mn should not be further reduced from trivalency, because of  $\text{Mn}^{2+}$  dissolving in the electrolyte [30,41,154,155]. Furthermore, Mn ion at trivalent state can undergo a disproportionation reaction forming  $\text{Mn}^{2+}$  and  $\text{Mn}^{4+}$  [83,156,157]. Due to the soluble nature of  $\text{Mn}^{2+}$ , when it is dissolved into the electrolyte, the active material gets lost. Subsequently,  $\text{Mn}^{4+}$  species forms on the surface. Since the  $\text{Mn}^{4+}$  cannot be electrochemically oxidised/charged, this leads to a loss of coulombic efficiency. Furthermore, on the anode, the dissolved  $\text{Mn}^{2+}$  ions can migrate to the anode side. The  $\text{Mn}^{2+}$  ions on the anode will reduce further down to the metallic state or form unwanted solid products and deposit on the anode surface. The deposited Mn species add electrochemical impedance that compromises battery performance.

### Solution

#### Morphology

In spite of the difficult control of the particle morphology *via* the solid-state method, the  $\text{LiMn}_2\text{O}_4$  is synthesised *via* solid-state method at the early stage of the research [149]. Since then, a wider range of wet-chemical approaches has been reported such as sol–gel and coprecipitation methods [158–160]. Employing the wet-chemical approach, the published particles are uniform in morphology and size and nano-sized particles improve the performance [161–166]. They have a large surface area for ion intercalation and short diffusion pathways for ion diffusion. While much effort has been made to synthesise the nanoscale  $\text{LiMn}_2\text{O}_4$ , only a few have studied the chemical implications of such morphologies. Zhao et al. adapted the hydrothermal reaction to synthesise nanowire morphology and coated the nanowire with a carbon material [167]. The bare nanowire exhibited faster performance decay in the low power cycling, however, it showed a good performance in the high power cycling. This study clearly indicated the instability of  $\text{LiMn}_2\text{O}_4$  nanowires. The Mn-containing systems are prone to undergo degradation involving lower oxidation states. Promoting high surface area can foster high-power performance while long-term stability can be compromised.

## Electrolyte

Unlike an organic electrolyte, an aqueous electrolyte behaves differently under electrochemical bias. Organic electrolyte molecules often decompose on the surface of the active materials upon electrochemical biasing. The decomposed molecules deposit on the surface of the active materials and form the solid-electrolyte interphase (SEI). The aqueous electrolyte, on the other hand, does not form such kind of layer (Figure 12). Instead, when the water electrolyses, it generates gas phases, which do not deposit on the surface of the active material [158]. In the organic LIB, the SEI layer has two main contributions: adding charge transfer resistance and electrode protection from the electrolyte. The charge transfer is hindered because  $\text{Li}^+$  from the electrolyte has to diffuse further distance to reach the redox active host. The advantage of the protective coating is that SEI creates a conformal coating around the active material. When  $\text{Li}^+$  ion is in the electrolyte, the ion is solvated and intercalates into the active material at the solvated stage. They can create strains in the crystal lattice that distort the crystal structure. Having the SEI layer can prevent unwanted ions from intercalating. Various ions can intercalate besides the  $\text{Li}^+$  including  $\text{H}^+$ ,  $\text{K}^+$ ,  $\text{Na}^+$ ,  $\text{NH}_4^+$ ,  $\text{Mg}^{2+}$ , and  $\text{Zn}^{2+}$  [168–171]. To protect the active material, conformal coating keeps Mn ion from dissolving into the electrolyte. The conformal coating provides protection for the active material and allows the electrode to last longer. Having the SEI layer increases the resistance to the electrode and helps to maintain the quality of the electrode longer.

The augmentation of the operating voltage span of aqueous electrolytes renders the aqueous LIB to be closer to real applications as a substitute for the high-power organic LIB (Figure 13(a)) [173]. Although the thermodynamic voltage stability window is only about 1.23 V, due to slow kinetic of water electrolysis, a practical voltage window is often wider than 1.23 V.

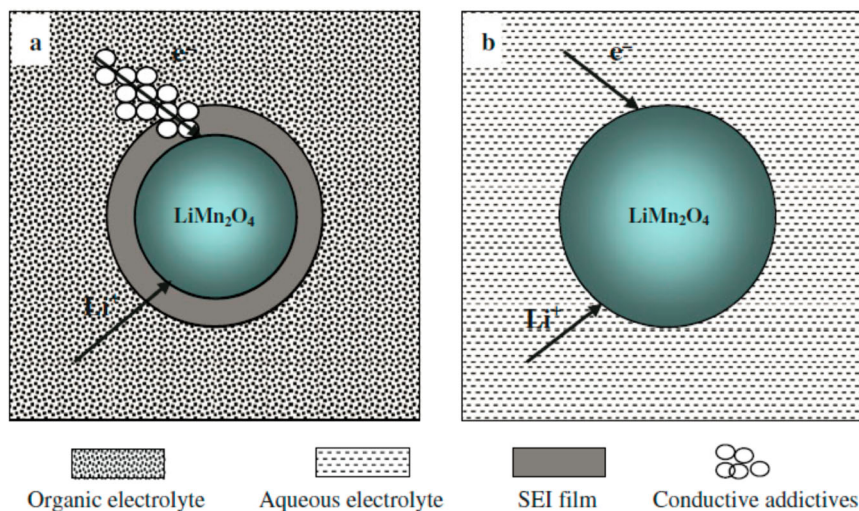


**Figure 12.** Schematic of (a) SEI formed active material in ORLB and (b) an active material in LIB [158].

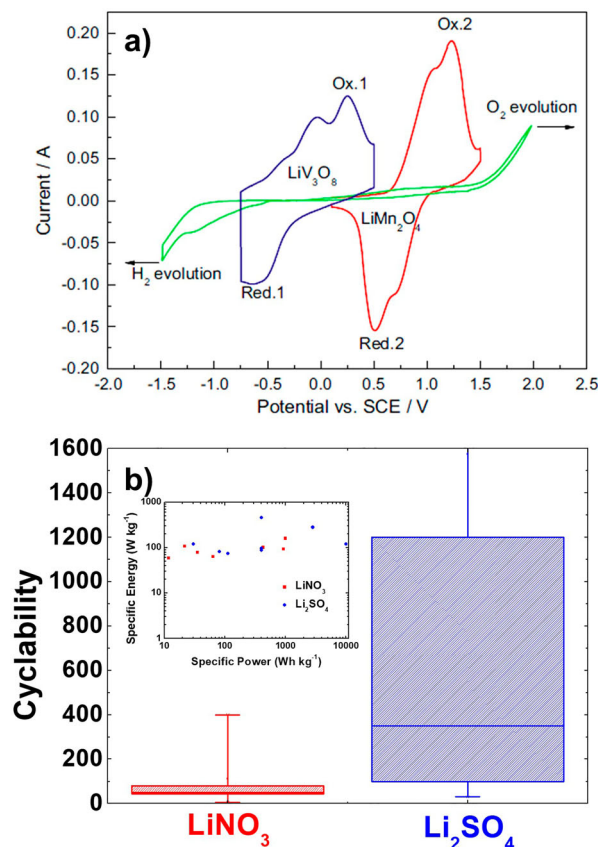


**Figure 13.** (a) Cyclic voltammetry of the  $\text{LiNO}_3$  electrolyte (green),  $\text{LiMn}_2\text{O}_4$  cathode (red), and  $\text{LiV}_3\text{O}_8$  anode (blue) in a LIB [172]. (b) Performance comparison of a LIB utilising either  $\text{LiNO}_3$  or  $\text{Li}_2\text{SO}_4$ . Source: Web of Science database. Data are updated on Jan 2018.

There are ways to expand the voltage stability window; One of them is employing a different type of Li salt because the kinetic of water electrolysis can be affected by the salt [174]. Some Li salt allows water to be stable in a broad voltage window. Compared to  $\text{Li}_2\text{ClO}_4$ ,  $\text{Li}_2\text{SO}_4$  exhibits better voltage stability of the electrolyte [173]. Both  $\text{LiNO}_3$  and  $\text{Li}_2\text{SO}_4$  are commonly used Li

salt for the aqueous electrolyte.  $\text{Li}_2\text{SO}_4$  shows better cyclability compared to  $\text{LiNO}_3$  (Figure 13(b)). In addition to the single salt system, a mixed salt system demonstrated to foster the performance as well [175,176]. The literature suggests various Li salts apply to the LIB, however, the mechanism of certain Li salt with different behaviour is not well explained. Understanding the role of Li salt in the kinetics of the electrolysis will help enlarge the water voltage window.

### Additive

Besides the active materials and the electrolyte with Li salt, there are additives that serve certain purposes to improve the performance overall. Because most of the intercalation active materials have low conductivity, the conductive additive is essential in many of the LIB electrodes [143]. One of the conductive additives is a conducting carbon material with a large surface area for electrical contact between the active materials and the current collector. Another way to implement the conductive additive is conformal coating around the active material. Having a layer on the surface of the active material helps to protect the Mn dissolution [172]. For example, when the nano-sized  $\text{LiMn}_2\text{O}_4$  is synthesised, it demonstrates a high rate electrochemical performance. In 2011, Zhao et al. proved that the sample quickly degraded when they conducted a low rate electrochemical test [177]. This indicates the material in the electrolyte is unstable. They coated the active material *via* the sucrose decomposition [178]. As a result, the carbon-coated sample had a longer cycle life and better electrochemical performance. It is widely accepted that those conductive additives do not participate in the electrochemical reactions, however, they act as a protective layer for an active material.

While some additives do not participate in the electrochemical reactions, there are other additives that actively engage in the electrochemical reactions. For instance, vinylene carbonate (VC), which can be added into the electrolyte, decomposes onto the surface of the active material and forms a stable solid coating layer [179]. The VC decomposition is kinetically preferred over the electrolyte decomposition [180]. Since the VC is more favourable to decompose, it quickly develops a stable coating layer before any damage is done to the active material. Mentus et al. have reported the use of VC in LIB in 2010 [181]. By applying the VC additive, they successfully stabilised the active material over prolonged cycles.

### Anode

For an electrochemical device, the full-cell property needs to be explained. The research in a half-cell is beneficial to gauge the intrinsic property of isolated electrode, however, a practical commercial cell should be

a full-cell with both electrodes of the electrochemical cell. Earlier in this section, optimising Li salt to widen the voltage window of the aqueous electrolyte was reviewed. If the voltage window was wider, it is possible to utilise a lower reduction potential anode, which brings out the stronger full-cell voltage, higher power, and greater energy output of the battery. Thus developing the electrolyte stability window must be accompanied with anode research. Much of the  $\text{LiMn}_2\text{O}_4$  cathode is countered with the vanadium-based anode. For example, the average voltage output was only about 1.1 V when it was utilised with vanadium-based anode [182]. Liu et al. successfully fabricated a LIB with  $\text{TiO}_2$  as an anode in 2011 [176]. They suppressed the electrolysis of water by mixing Li salt and utilising  $\text{LiCl}$  and  $\text{Li}_2\text{SO}_4$ . They achieved a high discharge voltage plateau of 2 V. Recently, even 4 V discharge voltage was reached by combining the concept of coating and voltage stability to the anode [183]. Normally, Li metal reacts spontaneously to water molecules to produce hydrogen gas, however, by coating Li with a  $\text{Li}^+$  ion conducting and water non-permeating solid film, Li metal can be used as an anode. Since  $\text{Li}/\text{Li}^+$  has  $-3.05$  V (vs. standard hydrogen electrode) reduction potential, the full-cell voltage dramatically rises.

### Na-ion battery

Aside from  $\text{Li}^+$  ion intercalation, there have been other cation intercalation mechanisms utilised in the manganese oxide system [184–186]. Especially, aqueous sodium-ion battery (NIB) has been studied extensively [187–192]. Among various NIB systems,  $\text{NaTi}_2(\text{PO}_4)_3/\text{Na}_{0.44}\text{MnO}_2$  (NTP/NMO) full cell is known to have the highest specific and volumetric energy density [193,194]. The NMO has an orthorhombic lattice with Pbam space group. It has double-tunnel crystal structure with corner sharing of edge-linked  $\text{MnO}_5$  square pyramids chains and  $\text{MnO}_6$  octahedral chains. The two types of tunnels are large S-shape tunnels, which are half-filled by  $\text{Na}^+$  ions, and small pentagonal tunnels that are fully occupied by  $\text{Na}^+$  ions. The Na ions located in S-shape tunnels can reversibly intercalate, projecting a theoretical capacity of  $\sim 50$  mAh  $\text{g}^{-1}$  (Figure 14(a)) [195]. This crystal structure greatly facilitates  $\text{Na}^+$  ion mobility while stabilising  $\text{Na}^+$  ions to prevent crystal phase transition to the spinel phase [196–198].

NMO cycling performance display drastically different phenomenon in non-aqueous to the aqueous electrolyte. In the non-aqueous electrolyte, Sauvage et al. describe that there is a drastic capacity fading at a rate higher than C/20 due to the sluggish phase transition kinetics [199]. Furthermore, Cao et al. calculated the  $\text{Na}^+$  ion diffusion coefficient to be around  $10^{-15}$ – $10^{-16}$   $\text{cm}^2 \text{ s}^{-1}$  [200]. On the other hand, in the aqueous electrolyte, the problem is in the low rates. Li et al.

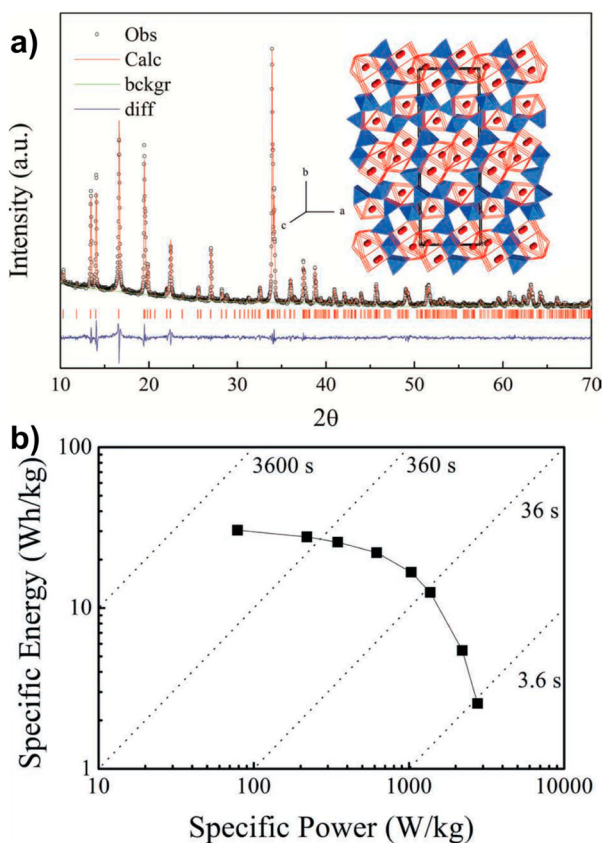


**Figure 14.** (a) Rietveld refinement of X-ray diffraction pattern of NMO and schematic illustration of crystal structure. (b) Ragone plot based on discharge energy and power obtained from NMO based full cell [195].

showed that the capacity fades at a rate lower than 1C due to the dissolution, oxidation of anodes, or oxidation of the electrolyte by the charged cathode [195]. Kim et al. also experimentally showed that the diffusion coefficient is two to three orders of magnitude higher in the aqueous electrolyte (aqueous:  $1.08 \times 10^{-13}$ – $9.18 \times 10^{-12}$   $\text{cm}^2 \text{s}^{-1}$  to non-aqueous:  $5.75 \times 10^{-16}$ – $2.14 \times 10^{-14}$   $\text{cm}^2 \text{s}^{-1}$  [201]). NMO in the aqueous electrolyte is capable of exceptionally high rates over 100C and stable cycling to >1000 cycles with materials only energy density of  $127 \text{ Wh L}^{-1}$  and cell-level density of  $\sim 65 \text{ Wh L}^{-1}$  [195]. NMO has abundant vacancies of  $\text{Na}^+$  ion diffusion in the S-shaped tunnel and possible strain accommodation during the intercalation reactions. Due to such high rate capability, NMO has been considered and utilised in the supercapacitor systems as well (Figure 14(b) [193,202–205]).

### Outlook

In this review, the current understanding of using  $\text{LiMn}_2\text{O}_4$  and  $\lambda\text{-MnO}_2$  as a cathode material in LIBs is explained. Much of the work in this field concentrates on synthesising the nano-sized materials. As it turns out, the nano-sized materials have instability concern at the interphase with the electrolyte. Instead

of the nano-sized materials, various forms of coating around the active material mechanically enhance the stability of the material. Since this material can be potentially used in the large-scale EESS, the stability of the material is essential. Although the literature provides several solutions: nano-sizing, expanding the water voltage window, coating, applying additives, and optimising anode, a systematic study to provide the optimum solution is scarce. Among numerous routes to improve the  $\text{LiMn}_2\text{O}_4$  performance, protecting the active materials from the electrolyte cannot be overlooked. It is needed to probe how these protections are mechanistically beneficial and propose the optimal material with the minimum charge transfer resistance while successfully protecting the active material. A deeper understanding of the mechanism will encourage the application of  $\text{LiMn}_2\text{O}_4$ .

## An air catalyst for metal-air batteries

### Introduction

There is a strong global incentive in developing EESS to alleviate the oil depletion and mitigate the greenhouse gas emission. LIBs have flourished in a variety of applications, however, high cost of manufacturing LIBs and limited energy density have kept LIBs from fully replacing fossil fuels. This motivates the research towards metal-air batteries (MAB). There are various metals (Zn, Li, Al, Ge, Ca, Fe, Mg, K, Na, Si, and Sn) that can be adopted as an anode for MABs [206,207]. Zn stands out in terms of safety, rechargeability, and the cost among a number of other candidates. The development of Zinc-air battery (ZAB) is relatively mature compared to other MABs with energy storage up to  $1080 \text{ Wh kg}^{-1}$  [208]. In fact, ZABs existed in the commercial market for over 40 years as a primary battery for hearing aid applications [22]. In MABs where  $\text{O}_2$  is employed as a cathode, oxygen reduction reaction (ORR) occurs during discharge and oxygen evolution reaction (OER) occurs at the cathode during charge. However, due to the sluggish nature of the oxygen reactions, there is a large overpotential (Figure 15(a)) [209].

The overpotential is related to the  $\text{O}_2$  adsorption onto the electrode surface and the cleavage of the  $\text{O}=\text{O}$  bond [211]. The overpotential greatly impedes the commercialisation of MABs because it lowers the energy efficiency of the battery [212]. To reduce the overpotential, cathode requires catalysts for reactions. There are many catalysts proposed in the literature, by and large, there are two main categories: metals and metal oxides. The volcano plot is a well-known method to represent the activity of an electrocatalyst, which reflects the Sabatier principle. This explains the optimal catalytic activity that can be achieved by the catalyst surface with respect to the appropriate binding energy for reactive intermediates [210].

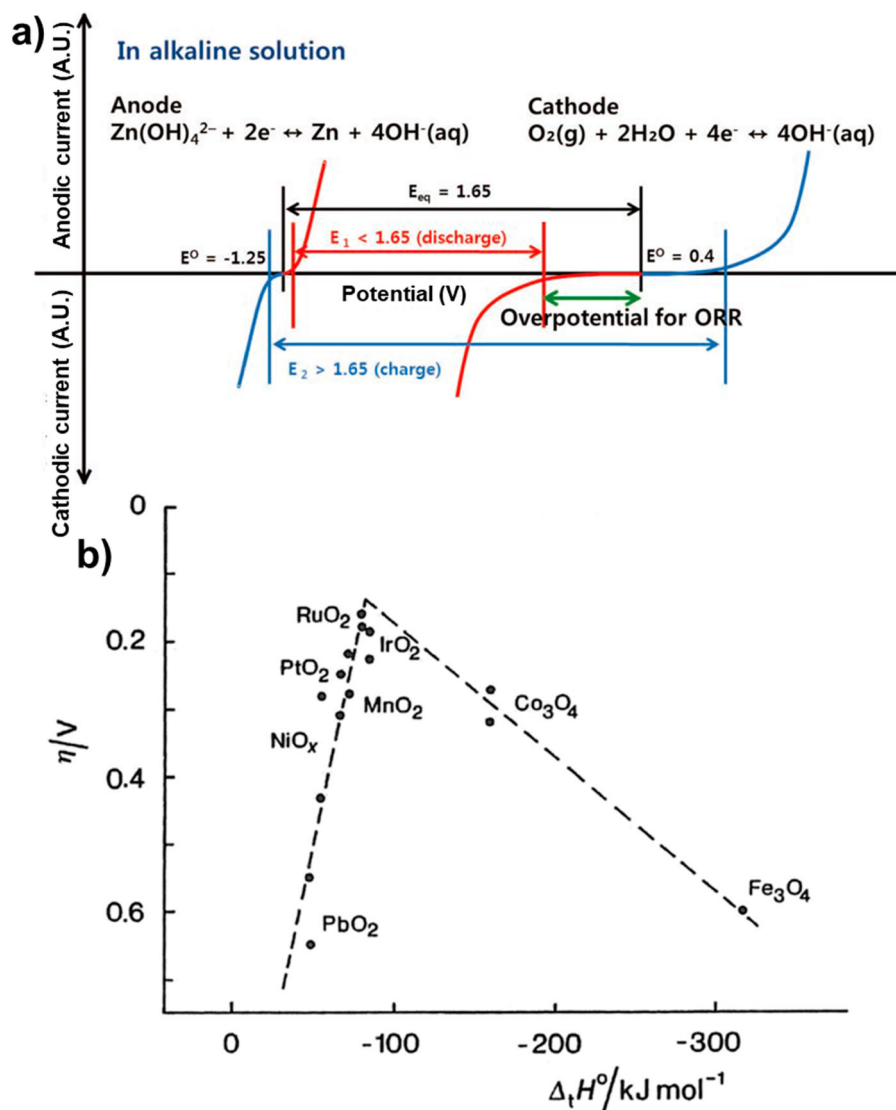


**Figure 15.** (a) Schematic polarisation curves of a zinc-air battery [209]. Reprinted with permission. Copyright 2011 Advanced Energy Materials. (b) Volcano plot of ORR activity designed as a function of the oxygen binding energy of metal oxides [210].

Optimum binding energy is required for a suitable electrocatalyst [213]. Among the catalysts, metals such as Pt, Pd, Ag, and Ir show high catalytic activity, but they are expensive [213]. On the other hand, metal oxides including  $\text{Co}_3\text{O}_4$ ,  $\text{LaNiO}_3$ ,  $\text{AB}_2\text{O}_4$  spinel structure (A is the divalent ions: Mg, Fe, Co, Ni, Mn, Zn, and B is the trivalent ions: Al, Fe, Co, Cr, and Mn), and Mn oxides with various oxidation states also show promising catalytic activities (Figure 15(b)) [210, 214–217].  $\text{MnO}_2$  is advantageous to other oxides because it has a high oxidation state and inexpensive to produce. In addition to  $\text{MnO}_2$ ,  $\text{MnOOH}$ ,  $\text{Mn}_5\text{O}_8$ , and  $\text{Mn}_2\text{O}_3$  have also demonstrated ORR catalytic activity in Mn oxide family [218,219].

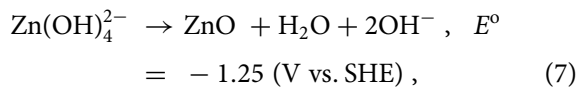
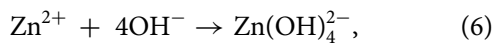
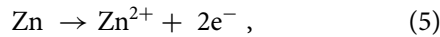
### History and mechanism

The invention of a ZAB originates in the nineteenth century [22]. Zoltowski et al. in 1973 proposed a mixture of  $\text{Mn}^{3+}$  and  $\text{Mn}^{2+}$  oxide compound [220]. At the early stage, the battery suffered from an electrolyte

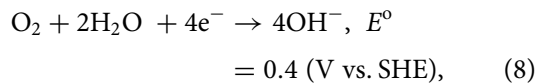
leakage and evaporation on the cathode side. With the development of highly controlled porosity of the teflon supportive hydrophobic film, the catalyst well adhered to the film surface while inhibiting the leakage [221]. Afterward,  $\lambda\text{-MnO}_2$  was used in the ZAB cell for the first Duracell hearing aid. By 1980s, ZABs have replaced carbon/zinc batteries and have become the majority of hearing aid's batteries [22]. ZABs are implemented into public transportation in 2012 after decades of efforts to prevent the dendritic growth of zinc to improve the catalytic activity and to package the cell safely. With the effort of scientists at Lawrence Livermore National Laboratory (LLNL), six 7 V ZABs empowered a bus to drive 75 miles without refueling [222].

There are three main types of ZABs: a primary battery, a mechanically rechargeable battery, and an electrochemically rechargeable battery. The primary battery utilises zinc as fuel until it is depleted [221]. The mechanism of the mechanically rechargeable ZAB is similar to the primary ZAB. The only difference

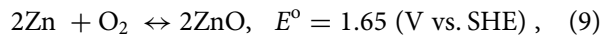
is that the Zn anode can be replaced once Zn is consumed. The electrochemically rechargeable ZAB can electrochemically restore Zn after depletion. For such kind of batteries, the catalyst on the cathode must be able to catalyse OER during charging. A typical ZAB encountering ORR and OER is summarised in Figure 16. The cell is comprised of a porous cathode, a membrane separator, and a zinc anode in an alkaline electrolyte. The Zn on the anode is oxidised during discharging.  $\text{Zn}^{2+}$  reacts to  $\text{OH}^-$  to form electrolyte and eventually stabilises to  $\text{ZnO}$ . The anode elementary reactions are as follows:



Simultaneously, oxygen on the cathode surface is reduced to hydroxide species *via* ORR. The cathode reaction is as follows:

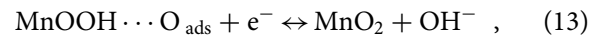
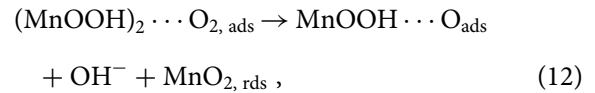


On the other hand, during charging,  $\text{ZnO}$  is reduced back to Zn at the anode and the hydroxide species is oxidised back to oxygen at the cathode *via* OER [223–225]. The overall reaction is as follows:

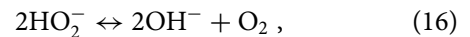


The overall oxygen reactions can be described in Equation (8) in which  $\text{H}_2\text{O}$  acts as a proton donor. The oxygen reduction mechanism can be broken down into two types [25]. The first type is called a

direct reduction reaction. The catalytic reduction of oxygen begins with inserting proton into  $\text{MnO}_2$ . This leads  $\text{Mn}^{4+}$  to partially reduce to  $\text{Mn}^{3+}$ . The oxygen molecule is adsorbed onto the  $\text{MnO}_2$  surface. Then the adsorbed oxygen molecule binds with hydrogen to form  $\text{OH}^-$  ions and diffuse back into the electrolyte. The elementary steps of the direct reduction reactions are as follows:



The other oxygen reduction mechanism is called an indirect reduction reaction. When the oxygen molecule is reduced with an electron without the presence of  $\text{MnO}_2$ ,  $\text{HO}_2^-$ , hydroperoxyl ion forms. The hydroperoxyl ion is an intermediate phase, which reduces to the hydroxide ion. However, the presence of hydroperoxyl ions in the electrolyte results in an unwanted corrosive effect on the cell. The elementary reaction steps are as follows:



On the other hand, OER occurs while the ZAB is being electrochemically recharged. OER catalytic reaction is induced by the interaction between metal ions and oxygen intermediates. The geometry of the metal cation site influences the catalysis process. It changes

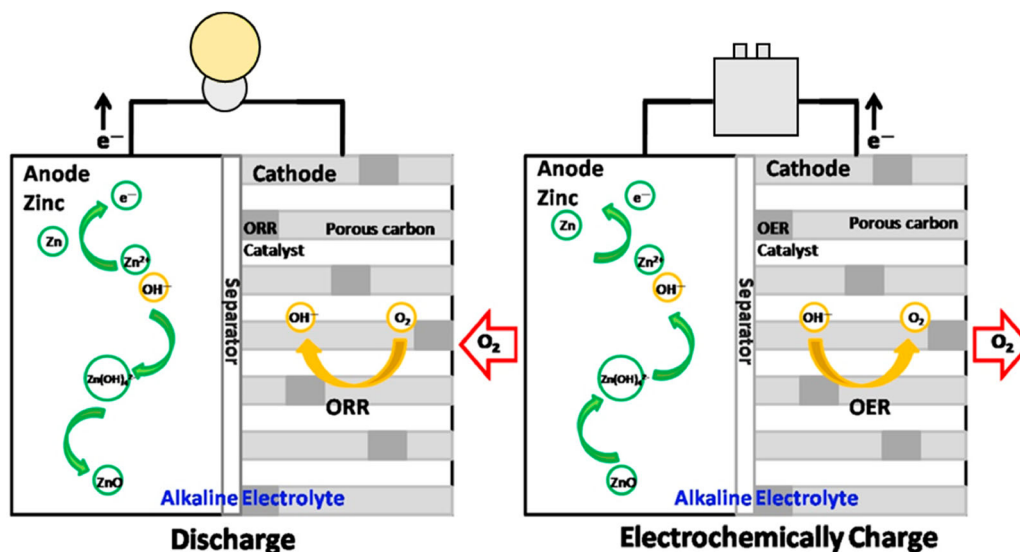
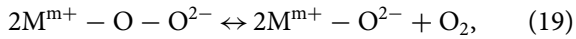
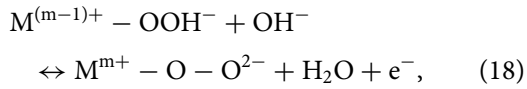
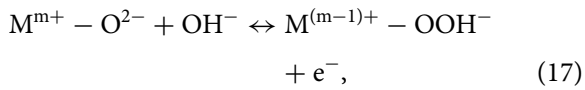


**Figure 16.** Graphical representation of the ORR (left) and OER (right) reactions of a ZAB during discharging and electrochemically charging with the reactions involved.

the adsorption energy of the oxygen species and the activation energy of the cation oxidation state [224,226]. For a rechargeable ZAB, OER occurs in alkaline solution with the following reaction [227]:



M refers to the cation ion of an OER catalyst. RuO<sub>2</sub> and IrO<sub>2</sub> have very high activity toward OER reactions due to their relatively low reduction potentials, 1.39 and 1.35 V vs. SHE, respectively and the high intrinsic conductivity [210,228]. MnO<sub>2</sub> is not being widely reported as an OER catalyst, yet α-Mn<sub>2</sub>O<sub>3</sub> is reported as a good bifunctional catalyst among the Mn oxides family [229].

### Bottleneck

A ZAB suffers from the high overpotential resulting from the sluggish oxygen reactions, which reduces power and energy efficiency [230]. Ample effort has been made to lower the overpotential by finding a proper catalyst and MnO<sub>2</sub> is considered as the most rewarding electrocatalyst, especially in the ORR (charging). However, MnO<sub>2</sub> still needs to be refined in two areas: enhancing the catalytic activity and stabilising against the corrosion for a battery to last longer. First, to boost the catalytic activity, an intrinsic property such as low electronic conductivity (10<sup>-5</sup>–10<sup>-6</sup> S cm<sup>-1</sup>) needs to be improved. The slow electronic transfer hinders a fast catalytic activity. Second, to stabilise against the corrosion, the indirect catalytic reaction should be suppressed. This reaction leads to H<sub>2</sub>O<sub>2</sub> and HO<sub>2</sub><sup>-</sup> formations and damages the catalyst. The corroded catalyst causes Mn ions to dissolve into the electrolyte and lose catalyst.

### Solutions

#### Polymorphs

The catalytic reaction occurs with the oxygen adsorption on the MnO<sub>2</sub> surface. The local environment for the oxygen adsorption varies depending on different polymorphs and it affects the catalytic activity. The local environment for oxygen adsorption varies for different polymorphs. There are reports comparing the various polymorphs to determine the optimum phase. The crystalline structures, chemical composition, morphology, and particle sizes are examined as a function of the electrocatalytic activity [231,232]. The ORR activity with respect to the various phases

of MnO<sub>2</sub> is in the following order: β < λ < γ < α ≅ δ-MnO<sub>2</sub> [219,233]. It is suggested that α-MnO<sub>2</sub> has the largest tunnel size than the rest of the MnO<sub>2</sub> polymorphs. The hydrogen insertion, which initiates the oxygen reduction, is promoted due to the large pore size. In addition, α-MnO<sub>2</sub> has a larger –OH terminated surface compared to the other polymorphs. This termination encourages the oxygen adsorption and dissociation of O–O bonds [9,234,235]. Upon the hydrogen insertion, oxygen begins to adsorb. It is also suggested that (310) surface has the highest affinity towards water adsorption [236]. By preferentially growing the crystal to expose more part of the (310) surface, the catalytic activity can be enhanced. [236–238].

#### Composite electrode

Although MnO<sub>2</sub> shows promising ORR activity, it is still limited to fully apply MnO<sub>2</sub> due to its low electrical conductivity. To overcome this problem, conductive carbon materials, such as carbon black, graphene, carbon nanotube, and katjen black are commonly mixed to make the composite electrode [211,229,239–243]. Aside from these electrochemically inactive and conductive carbon materials, there are composite materials actively involved in the electrochemistry. Most of the catalytic activities of MnO<sub>2</sub> focus on the ORR, thus the OER has not been highlighted until recently. The OER is enabled by utilising composite electrodes. When MnO<sub>2</sub> is mixed with another spinel, perovskite, or pyrochlore structure (CO<sub>3</sub>O<sub>4</sub>, La<sub>2</sub>O<sub>3</sub>, LaNiO<sub>3</sub>, or LaMnO<sub>3</sub>), the ORR and OER activity and the stability improved [244–247]. Goujun et al. demonstrated 60 cycles of ORR/OER retention with a nanotube of MnO<sub>2</sub>/Co<sub>3</sub>O<sub>4</sub> composite electrode [248]. Co–Mn–O spinel compound synthesised from δ-MnO<sub>2</sub> nanoparticle as a precursor facilitated the ORR/OER [249]. An electrode made by Golin et al. adopted only Mn oxide [229] whereas the assistance of none-Mn-based oxides facilitated the OER activity. Their Mn oxide electrode is a mixed phase of Mn<sup>3+</sup> and Mn<sup>4+</sup>. Regardless, this electrode, namely bifunctional electrode, shows both ORR and OER activities.

#### Doping

Fabricating the composite electrode enhances ORR and OER activity by mixing an ORR catalyst and an OER catalyst. On the other hand, doping encourages both reactions with a single catalyst and directly alters the intrinsic catalytic activity of MnO<sub>2</sub> without inserting extra additives [250,251]. There are two doping positions in MnO<sub>2</sub>: (1) doping lower-valent ions in the place of Mn ions and (2) doping alkali metal cations in the pores of MnO<sub>2</sub>. In the first doping position, MnO<sub>x</sub> doped with Ni<sup>2+</sup> and Mg<sup>2+</sup> exhibited better catalytic performance than the pristine MnO<sub>2</sub> in alkaline medium [241]. Roche et al. suggested that with the

presence of  $\text{Ni}^{2+}$  and  $\text{Mg}^{2+}$ , the peroxide production is significantly suppressed [241]. This is accomplished by keeping Mn at a higher oxidation state. At the same time,  $\text{Mn}^{3+}$  dissolution is prevented because of maintaining Mn at a higher oxidation state. Quimei et al. demonstrated that the  $\text{Ni}^{2+}$  doped  $\text{MnO}_x/\text{C}$  composite delivered the power density of  $122 \text{ mW cm}^{-2}$  in a primary ZAB, which is comparable to Pd/C and Pt/C catalysts [252]. However, not all the divalent dopants make a positive impact on the catalytic activity of the  $\text{MnO}_2$  compound.  $\text{Ca}^{2+}$ , as an example, leads to a lower ORR current. With the presence of  $\text{Ca}^{2+}$ ,  $\text{MnO}_2$  reduces to  $\text{Mn}_5\text{O}_8$ , which is an electrochemically unfavourable compound. Further studies are required to understand the optimum dopants.

Another doping position dopes alkali metal cations inside the pores of  $\text{MnO}_2$ . Lee et al. introduced Na to  $\alpha\text{-MnO}_2$  nanowire through a hydrothermal synthesis and introduced defects to the structure through acid leaching. The defects in the  $\text{Na}_{0.44}\text{MnO}_2$  nanowire diminished the OER overpotential [253]. In addition to Na,  $\alpha\text{-MnO}_2$  can be doped with Li and K cations [254]. Doping these alkali metal cations alters the electronic structure of Mn. Doping  $\text{MnO}_2$  can bridge the band gap, which allows a faster electronic transfer. The same doping can also be applied to  $\delta\text{-MnO}_2$ : K, Na, Bi, Ni, and Al cations [255–257]. The doping effect of those cations is accomplished by changing the stacking structure, lowering the band gap, and decreasing the charge transfer resistance.

### Structural defect

The formation of the  $\text{Mn}_5\text{O}_8$  phase is not favoured in the electrochemical performance. Mao et al. suggested that the rate of electrochemical activity of  $\text{MnO}_x$  complexes is as follows:  $\text{Mn}_5\text{O}_8 < \text{Mn}_3\text{O}_4 < \text{Mn}_2\text{O}_3 < \text{MnOOH}$  [218,219,258]. Among the mixed valent Mn oxides, MnOOH produces the highest catalytic activity. Furthermore, Matsuki et al. enhanced the activity by heat treating MnOOH and distorting the crystal structure [258], which enlarges the activation sites and boosts the activity. For  $\text{MnO}_2$ , it is pointed out that the phase of  $\text{MnO}_2$  plays a crucial role in adsorbing oxygen. Distorting the crystal structure of  $\text{MnO}_2$  also helps to adsorb the oxygen. When the pristine  $\beta\text{-MnO}_2$  is heat treated in both Ar and air, an oxygen vacancy is created [259]. Introducing an oxygen vacancy is another way to absorb more oxygen. An oxygen vacancy implemented to  $\beta\text{-MnO}_2$  structure helps the catalytic activity, however, the vacancy is compensated by reducing  $\text{Mn}^{4+}$ . They also claimed that the hydrogen peroxide formation was suppressed during the ORR.

### Morphology

The difference in morphology can play important roles in ORR and OER activity of a  $\text{MnO}_2$  catalyst due to the

related surface area and the exposed facets of a catalyst, which in turn can tune the catalytic behaviour. The morphology of the end-product typically depends on the chemical reaction conditions such as temperature, the concentration of reactants, and the reaction time [219]. Cheng et al. show that the catalytic activity of  $\alpha\text{-MnO}_2$  can be different with different morphology of the synthesised product. The nanoflower structure shows higher catalytic activity than the nanowire structure and the bulk structure. This is due to the nanoflower structure processes more defects and has more hydroxyl groups, leading to the high exposed surface area. As a result, induced higher oxygen reduction potential and larger current density (as shown in Figure 17) [260]. Moreover, the same group fabricated nanocrystalline  $\text{Co}_x\text{Mn}_{3-x}\text{O}_4$  spinel with amorphous  $\text{MnO}_2$  precursors with a hope to tune the morphology to a broader range such as nanowires, nanoflakes, and nanoflower structures and to result into a higher catalytic activity [249]. Later on, Li et al. show that through a co-precipitation method can lead to different disperse of  $\text{MnO}_2/\text{CNT}/\text{Co}_3\text{O}_4$  structure and it influences the catalytic activity as well. Generally, a more discrete synthesised powder can lead to a better ORR/OER activity [261]. Meng et al. also shows that with different synthesis routes, the resulting behaviour of  $\text{MnO}_2/\text{CNT}$  will be different. They show that with a small width but larger length  $\text{MnO}_2/\text{CNT}$  can result in a higher ORR/OER efficiency than the bulk  $\alpha\text{-MnO}_2$ . It is due to the improved thermostability and bonding efficiency to  $\text{O}_2$  due to the solvent-free synthesis [262].

### Electrocatalytic applications

The ZAB has demonstrated promising ORR and OER activity of a  $\text{MnO}_2$  catalyst. Utilising the OER activity, the  $\text{MnO}_2$  catalyst can have a number of additional applications. For instance, fuel cells that utilise ORR reactions suffer from high Pt catalyst cost. By replacing the Pt catalyst with  $\text{MnO}_2$  catalyst can dramatically drive down the cost of fuel cells [263,264]. Furthermore, the hydrogen, fuel for the fuel cell, can be generated *via* electrolysis water molecules. This sluggish electrolysis reaction also requires an efficient catalyst. The  $\text{MnO}_2$  has been shown to assist in the hydrogen evolution reaction (HER) and OER which improves the electrolysis systems [265,266]. Besides the reactions involving oxygen,  $\text{MnO}_2$  catalyst has been utilised in various other fields including CO oxidation [267], methanol oxidation [268], photocatalyst [269], etc.

### Outlook

In this section, adopting  $\text{MnO}_2$  as a MAB catalyst is discussed. The majority of the work in this field mainly focuses on mixing or doping foreign elements to enhance the catalytic activity, however, the durability of those catalysts in a practical ZAB remains unclear.

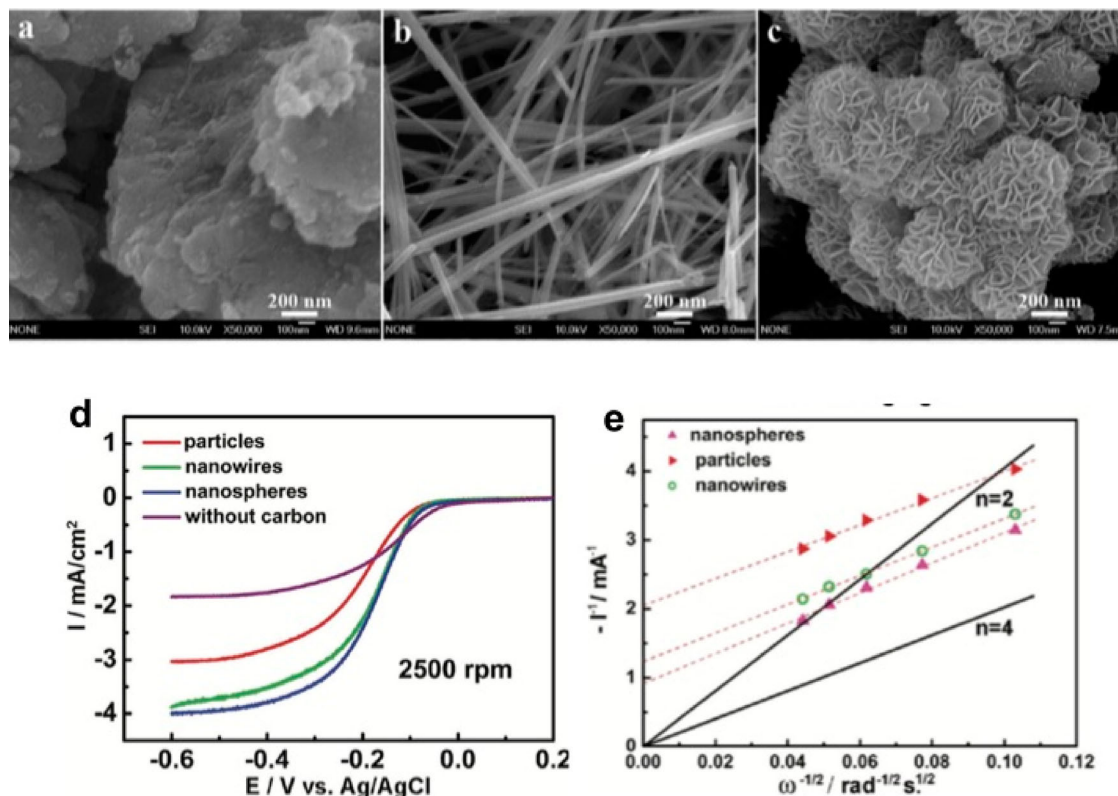


**Figure 17.** Morphology change with different preparation conditions and resulted in (a) bulk particles (b) nanowires (c) flower-like  $\alpha$ -MnO<sub>2</sub> structures. The catalytic activity is shown in (d) LSV comparison and (e) the corresponding K–L plot [260]. Reprinted with permission. Copyright 2009 Chemistry of Materials.

Most of the optimum performances originate from nano-sized and thin film electrodes. With such kind of electrodes, the stability of the electrode at the electrolyte interphase can be a concern. Golin et al. reported that after the catalytic activity, their Mn oxide electrode did not turn back to its pristine state [270]. A catalyst material is a critical issue for a ZAB since it influences the overpotential. When the integrity of the catalyst is compromised, the overall performance of ZAB is sacrificed.

### Future directions

In this review, we have provided extensive reports on comprehensive mechanistic understanding of MnO<sub>2</sub> in alkaline batteries, supercapacitors, LIB, and MAB systems. Despite the long history and an enormous number of reports, the MnO<sub>2</sub> systems are still far from commercialisation. We have described the alkaline system as the system with the longest history and the others as the systems with exponential interest. Due to intense crystallographic research before 1995, the phase transformation of MnO<sub>2</sub> in the alkaline system has been well understood [43]. Various additive research has identified some key functional materials to promote reversible phase formations and hinder irreversible phase formations. On the other hand, the other systems have exponential growth of interest. Various nanostructures are synthesised and materials are

coated through novel techniques. Nevertheless, much of the reports are missing some key information such as phase identification, hydrogen location, the role of additives, etc. For further developing the MnO<sub>2</sub> systems as the EESSs and ultimately commercialising, more efforts should be paid to characterisation. In the authors' perspective, several promising directions can be generalised as follows.

### Hydrogen involvement

We have repeatedly emphasised that phase differentiation is one of the starting stages of comprehensive research in MnO<sub>2</sub> systems. Although an in-depth understanding of the phase transformation in the alkaline system is available, with the recent advancement of the characterisation tools, further information can be obtained. Especially when the systems utilise aqueous electrolyte, there are hydrogen atoms involved in the electrochemical reactions. Although much of the available reports obtained crystal information through X-ray source, the X-ray source is not an adequate source to detect hydrogen. To identify the exact crystallographic location of the hydrogen atom, the neutron source must be utilised [271]. Identifying the hydrogen location achieves true phase identification and ultimately assists in the kinetic understanding of the phase transformation. Furthermore, applying neutron source can also identify the location of the Li<sup>+</sup> ions.

For the LIB, it is crucial to distinguish the lithium intercalation from the hydrogen intercalation.

### In situ characterisation

To comprehend a full phase transformation during the electrochemical cycle, the pristine characterisation does not provide a sufficient amount of information. Reports on *ex situ* studies are available and they identify thermodynamically stable phases. On the other hand, *in situ* or *operando* studies are scarce, yet these experimental settings provide kinetically stable phases [272,273]. Kinetically stable phases provide information on the intermediate reactions. When a phase transformation occurs, the intermediate phase allows us to understand how atoms are rearranging. This helps to identify which phase transformations impose higher atomic strain or stress and relate this to  $\text{Mn}^{2+}$  dissociation. MAB system can obtain vital information because an enormous number of MAB studies report improved catalytic activity, but the degradation mechanism is scarce. *In situ* characterisation during chronoamperometry experiment can shed light on the durability of the MAB system. Constructing such a sophisticated experimental setting is especially involved for supercapacitor systems. Because supercapacitor charge and discharge processes take only a few seconds to finish, common characterisation tools are not suitable to capture the kinetic information. As an example, quick-scanning X-ray absorption fine structure (QXAFS) is one of the few characterisation tools that can detect chemical information within seconds [274]. QXAFS coupled with *operando* charge and discharge of the supercapacitor system can provide true redox mechanism.

### Computation assisted novel materials

Based on the thorough interpretation of the mechanism, numerous methods are applied to improve electrochemical performance. The routes discussed in this review are additives, coating/deposition, and doping/defect. While novel materials need to be applied, exploring these routes require screening [275]. Since searching every possible solution can take too much time and effort, first principles high-throughput computation methods should be utilised to find promising materials [276,277]. In order to perform the high-throughput screening, different traits of the potential property need to be established. For instance, the exact location of hydrogen needs to be known to construct a proper model and intermediate phases should be considered in the reaction scheme. Through considering these parameters, new materials can be proposed minimising the unnecessary syntheses [277,278].

### Conclusion

$\text{MnO}_2$  is an extremely inexpensive material and it is suitable for large-scale EESS. The four fields in discussion complement each other in the EESS as they output different range of power and energy performances. Current understanding and progress of four EESS systems using  $\text{MnO}_2$  are discussed in this review. Both alkaline battery and the LIB systems utilise intercalation reactions, yet different ions are intercalated to each of them. The alkaline battery field shows that additives selectively form desirable phases. The LIB field protects active materials through a surface coating. A supercapacitor and the MAB both utilise the surface of  $\text{MnO}_2$ , yet the surface reactions are different. The supercapacitor field exhibits various nano electrodes with a wide surface area and mass loading. The MAB field shows doping and defects to alter the electronic structure. The approaches in four EESS systems are diverse due to their differences in mechanisms, however, there are research pathways that share some common grounds. They all share two bottlenecks: (1) lack of conductivity and (2) an unwanted disproportionation reaction, which leads to dissolution. By probing exact material properties of EESS, comprehensive mechanisms can be developed. Although  $\text{MnO}_2$  has been studied for a long time and a lot of it is understood, with the recent advancement in the characterisation tools, new insights are waiting to be discovered.

### Disclosure statement

No potential conflict of interest was reported by the authors.

### Funding

The authors are grateful for the financial support in part by the Advanced Research Projects Agency-Energy (ARPA-E), U.S. Department of Energy; [grant number DE-AR0000535], the USA National Science Foundation; [grant number DMR1608968] and the Materials Science Fellowship at the University of California, San Diego.

### ORCID

Jaewook Shin  <http://orcid.org/0000-0002-7431-9255>

### References

- [1] Dunn B, Kamath H, Tarascon JM. Electrical energy storage for the grid: a battery of choices. *Science*. 2011;334(6058):928–935. DOI:10.1126/science.1212741. PubMed PMID: ISI:000297101800043; English.
- [2] EPRI-DOE handbook of energy storage for transmission and distribution applications. Palo Alto: EPRI and the U.S. Department of Energy; 2003.
- [3] Deane JP, Gallachoir BPO, McKeogh EJ. Techno-economic review of existing and new pumped hydro energy storage plant. *Renewable Sustainable*

- Energy Rev. 2010;14(4):1293–1302. DOI:10.1016/j.rser.2009.11.015. PubMed PMID: ISI:000275997200013; English.
- [4] Johnson CS. Development and utility of manganese oxides as cathodes in lithium batteries. *J Power Sources*. 2007;165(2):559–565. PubMed PMID: WOS:000245369100009; English.
- [5] Jarvis SC. The association of cobalt with easily reducible manganese in some acidic permanent grassland soils. *J Soil Sci*. 1984;35(3):431–438. PubMed PMID: ISI:A1984TL53800009; English.
- [6] Mckeague JA, Damman AWH, Heringa PK. Iron-manganese and other pans in some soils of Newfoundland. *Can J Soil Sci*. 1968;48(3):243–224. PubMed PMID: ISI:A1968C027800003; English.
- [7] Mckenzie RM. Synthesis of birnessite, cryptomelane, and some other oxides and hydroxides of manganese. *Mineral Mag*. 1971;38(296):493–449. DOI:10.1180/minmag.1971.038.296.12. PubMed PMID: ISI:A1971L205200012; English.
- [8] Julien CM, Massot M, Poinignon C. Lattice vibrations of manganese oxides: part I. Periodic structures. *Spectrochim Acta, Part A*. 2004;60(3):689–700. DOI:10.1016/S1386-1425(03)00279-8.
- [9] Thackeray MM. Manganese oxides for lithium batteries. *Prog Solid State Chem*. 1997;25(1–2):1–71. DOI:10.1016/S0079-6786(97)81003-5.
- [10] Su D, Ahn HJ, Wang G. Hydrothermal synthesis of  $\alpha$ - $\text{MnO}_2$  and  $\beta$ - $\text{MnO}_2$  nanorods as high capacity cathode materials for sodium ion batteries. *J Mater Chem A*. 2013;1(15):4845–4850. DOI:10.1039/c3ta00031a. PubMed PMID: ISI:000316282800030; English.
- [11] Julien C, Massot M, Rangan S, et al. Study of structural defects in  $\gamma$ - $\text{MnO}_2$  by Raman spectroscopy. *J Raman Spectrosc*. 2002;33(4):223–228. DOI:10.1002/jrs.838.
- [12] Herbert WS. Fiftieth anniversary: the anniversary issue on primary cell systems: the alkaline manganese dioxide dry cell. *J Electrochem Soc*. 1952;99(8):190C–191C. DOI:10.1149/1.2779731.
- [13] Gallaway JW, Menard M, Hertzberg B, et al. Hetaerolite profiles in alkaline batteries measured by high energy EDXRD. *J Electrochem Soc*. 2015;162(1):A162–A168. DOI:10.1149/2.0811501jes.
- [14] Chen H, Cong TN, Yang W, et al. Progress in electrical energy storage system: a critical review. *Prog Nat Sci*. 2009;19(3):291–312. DOI:10.1016/j.pnsc.2008.07.014.
- [15] Chao D, Zhou W, Ye C, et al. An electrolytic Zn– $\text{MnO}_2$  battery for high-voltage and scalable energy storage. *Angew Chem Int Ed*. 2019;58(23):7823–7828. DOI:10.1002/anie.201904174.
- [16] Kundu D, Adams BD, Duffort V, et al. A high-capacity and long-life aqueous rechargeable zinc battery using a metal oxide intercalation cathode. *Nat Energy*. 2016;1:16119. PubMed PMID: WOS:000394182900001; English.
- [17] Minakshi M. Alkaline-earth oxide modified  $\text{MnO}_2$  cathode: enhanced performance in an aqueous rechargeable battery. *Ind Eng Chem Res*. 2011;50(14):8792–8795. DOI:10.1021/ie2001742.
- [18] Yadav GG, Gallaway JW, Turney DE, et al. Regenerable Cu-intercalated  $\text{MnO}_2$  layered cathode for highly cyclable energy dense batteries. *Nat Commun*. 2017;8:14424. DOI:10.1038/ncomms14424. <http://www.nature.com/articles/ncomms14424#supplementary-information>.
- [19] Pan H, Shao Y, Yan P, et al. Reversible aqueous zinc/manganese oxide energy storage from conversion reactions. *Nat Energy*. 2016;1:16039.
- [20] Turney DE, Gallaway JW, Yadav GG, et al. Rechargeable zinc alkaline anodes for long-cycle energy storage. *Chem Mater*. 2017;29(11):4819–4832. DOI:10.1021/acs.chemmater.7b00754.
- [21] Chabre Y, Pannetier J. Structural and electrochemical properties of the proton/ $\gamma$ - $\text{MnO}_2$  system. *Prog Solid State Chem*. 1995;23(1):1–130. DOI:10.1016/0079-6786(94)00005-2.
- [22] Linden D, Reddy TB. Handbook of batteries. 3rd. New York: McGraw-Hill; 2002.
- [23] Leuchs G. inventor. German Pat. 24552.
- [24] Yai S. inventor. U. S. Pat. 746227.
- [25] Achenbach E. inventor. German Pat. 261319.
- [26] Karl K, Marsal PA, Urry LF. inventors; Google Patents, assignee. Dry cell patent US2960558 A. 1960.
- [27] McBreen J. The electrochemistry of  $\beta$ - $\text{MnO}_2$  and  $\gamma$ - $\text{MnO}_2$  in alkaline electrolyte. *Electrochim Acta*. 1975;20(3):221–225. DOI:10.1016/0013-4686(75)85028-6.
- [28] Boden D, Venuto CJ, Wisler D, et al. The alkaline manganese dioxide electrode. *J Electrochem Soc*. 1967;114(5):415–417. DOI:10.1149/1.2426618.
- [29] Holton D, Maskell W, Tye F. Power Sources 10' (edited by L. Pearee). London: The Paul Press; 1985.
- [30] Minakshi M, Singh P. Synergistic effect of additives on electrochemical properties of  $\text{MnO}_2$  cathode in aqueous rechargeable batteries. *J Solid State Electrochem*. 2012;16(4):1487–1492. PubMed PMID: WOS:000301983300022; English.
- [31] Kloß M, Rahner D, Plieth W. The effect of alkaline earth titanates on the rechargeability of manganese dioxide in alkaline electrolyte. *J Power Sources*. 1997;69(1–2):137–143..
- [32] Im D, Manthiram A. Role of bismuth and factors influencing the formation of  $\text{Mn}_3\text{O}_4$  in rechargeable alkaline batteries based on bismuth-containing manganese oxides. *J Electrochem Soc*. 2003;150(1):A68–A73. DOI:10.1149/1.1524611.
- [33] Minakshi M, Nallathamby K, Mitchell DRG. Electrochemical characterization of an aqueous lithium rechargeable battery: the effect of  $\text{CeO}_2$  additions to the  $\text{MnO}_2$  cathode. *J Alloys Compd*. 2009;479(1–2):87–90. PubMed PMID: WOS:000267063300036; English.
- [34] Bailey MR, Denman JA, Donne SW. Electrode additives and the rechargeability of the alkaline manganese dioxide cathode. *J Electrochem Soc*. 2014;161(3):A403–A409. DOI:10.1149/2.053403jes.
- [35] Karami H, Ghamooshi-Ramandi M. Pulse galvanostatic synthesis of zinc-sulfur nanocomposites and application as a novel negative material of rechargeable zinc-manganese dioxide alkaline batteries. *Int J Electrochem Sci*. 2012;7(3):2091–2108. PubMed PMID: WOS:000302730300029; English.
- [36] Kozawa A, Yeager JF. The cathodic reduction mechanism of electrolytic manganese dioxide in alkaline electrolyte. *J Electrochem Soc*. 1965;112(10):959–963. DOI:10.1149/1.2423350.
- [37] Minakshi M, Singh P, Carter M, et al. The Zn– $\text{MnO}_2$  battery: The influence of aqueous  $\text{LiOH}$  and  $\text{KOH}$  electrolytes on the intercalation mechanism. *Electrochem Solid-State Lett*. 2008;11(8):A145–A149. DOI:10.1149/1.2932056. PubMed PMID: WOS:000256706100006; English.

- [38] Motsegood PN. Improved performance of alkaline batteries via magnetic modification and voltammetric detection of breath acetone at platinum electrodes. 2012.
- [39] Ingale ND, Gallaway JW, Nyce M, et al. Rechargeability and economic aspects of alkaline zinc-manganese dioxide cells for electrical storage and load leveling. *J Power Sources*. 2015;276(0):7–18. DOI:10.1016/j.jpowsour.2014.11.010.
- [40] Ruetschi P, Giovanoli R. Cation vacancies in  $\text{MnO}_2$  and their influence on electrochemical reactivity. *J Electrochem Soc*. 1988;135(11):2663–2669. DOI:10.1149/1.2095406.
- [41] Kozawa A, Powers RA. Cathodic polarization of the manganese dioxide electrode in alkaline electrolytes. *J Electrochem Soc*. 1968;115(2):122–126. DOI:10.1149/1.2411042.
- [42] Minakshi M, Blackford M, Ionescu M. Characterization of alkaline-earth oxide additions to the  $\text{MnO}_2$  cathode in an aqueous secondary battery. *J Alloys Compd*. 2011;509(20):5974–5980. DOI:10.1016/j.jallcom.2011.03.044.
- [43] Kordesch K, Gsellmann J, Tomantschger K. The alkaline manganese dioxide-zinc cell. *J Electroanal Chem Interfacial Electrochem*. 1981;118(0):187–201. DOI:10.1016/S0022-0728(81)80540-2.
- [44] Patrice R, Gerand B, Leriche JB, et al. Understanding the second electron discharge plateau in  $\text{MnO}_2$ -based alkaline cells. *J Electrochem Soc*. 2001;148(5):A448–A455. DOI:10.1149/1.1362539. PubMed PMID: ISI:000168421200009; English.
- [45] Benjamin J, Hertzberg AH, Hsieh A, et al. The effect of binary electrolyte mixtures on rechargeable Zn- $\text{MnO}_2$  alkaline battery. Manuscript under Preparation. 2015.
- [46] Kozawa A, Kalnoki-Kis T, Yeager JF. Solubilities of Mn(II) and Mn(III) ions in concentrated alkaline solutions. *J Electrochem Soc*. 1966;113(5):405–409. DOI:10.1149/1.2423984.
- [47] Mondoloni C, Laborde M, Rioux J, et al. Rechargeable alkaline manganese dioxide batteries. *J Electrochem Soc*. 1992;139(4):954–959. DOI:10.1149/1.2069374.
- [48] Shin J, You JM, Lee JZ, et al. Deposition of ZnO on bismuth species towards a rechargeable Zn-based aqueous battery. *Phys Chem Chem Phys*. 2016;18(38):26376–26382. DOI:10.1039/c6cp04566a. PubMed PMID: ISI:000385175000005; English.
- [49] Hertzberg BJ, Huang A, Hsieh A, et al. Effect of multiple cation electrolyte mixtures on rechargeable Zn- $\text{MnO}_2$  alkaline battery. *Chem Mater*. 2016;28(13):4536–4545. DOI:10.1021/acs.chemmater.6b00232.
- [50] Huang J, Yadav GG, Gallaway JW, et al. A calcium hydroxide interlayer as a selective separator for rechargeable alkaline Zn/ $\text{MnO}_2$  batteries. *Electrochem Commun*. 2017;81(Supplement C):136–140. DOI:10.1016/j.elecom.2017.06.020.
- [51] Bailey MR, Donne SW. The effect of barium hydroxide on the rechargeable performance of alkaline  $\gamma$ - $\text{MnO}_2$ . *J Electrochem Soc*. 2012;159(7):A999–A1004. DOI:10.1149/2.047207jes.
- [52] Raghuvver V, Manthiram A. Effect of  $\text{BaBiO}_3$  and  $\text{Ba}_{0.6}\text{K}_{0.4}\text{BiO}_3$  additives on the rechargeability of manganese oxide cathodes in alkaline cells. *Electrochem Commun*. 2005;7(12):1329–1332. PubMed PMID: WOS:000233720500026; English.
- [53] Pan JQ, Sun YZ, Wan PY, et al. Preparation of  $\text{NaBiO}_3$  and the electrochemical characteristic of manganese dioxide doped with  $\text{NaBiO}_3$ . *Electrochim Acta*. 2006;51(15):3118–3124. PubMed PMID: WOS:000236845200018; English.
- [54] Seo JK, Shin J, Chung H, et al. Intercalation and conversion reactions of nanosized  $\beta$ - $\text{MnO}_2$  cathode in the secondary Zn/ $\text{MnO}_2$  alkaline battery. *J Phys Chem C*. 2018;122(21):11177–11185. PubMed PMID: WOS:000434236700001; English.
- [55] Wang Q, Pan JQ, Sun YZ, et al. A high capacity cathode material- $\text{MnO}_2$  doped with nano  $\text{Ag}_4\text{Bi}_2\text{O}_5$  for alkaline secondary batteries. *J Power Sources*. 2012;199:355–359. PubMed PMID: WOS:000298269700051; English.
- [56] Yadav GG, Wei X, Huang JC, et al. Accessing the second electron capacity of  $\text{MnO}_2$  by exploring complexation and intercalation reactions in energy dense alkaline batteries. *Int J Hydrogen Energy*. 2018;43(17):8480–8487. PubMed PMID: WOS:000431747600029; English.
- [57] Minakshi M, Mitchell DRG. The influence of bismuth oxide doping on the rechargeability of aqueous cells using  $\text{MnO}_2$  cathode and LiOH electrolyte. *Electrochim Acta*. 2008;53(22):6323–6327. DOI:10.1016/j.electacta.2008.04.013.
- [58] Gallaway JW, Gaikwad AM, Hertzberg B, et al. An in situ synchrotron study of zinc anode planarization by a bismuth additive. *J Electrochem Soc*. 2014;161(3):A275–A284. PubMed PMID: WOS:000332137100009; English.
- [59] Minakshi M, Blackford MG. Electrochemical characteristics of B4C or BN added  $\text{MnO}_2$  cathode material for alkaline batteries. *Mater Chem Phys*. 2010;123(2–3):700–705. PubMed PMID: WOS:000281175500060; English.
- [60] Minakshi M, Blackford MG, Thorogood GJ, et al. The effect of B4C addition to  $\text{MnO}_2$  in a cathode material for battery applications. *Electrochim Acta*. 2010;55(3):1028–1033. PubMed PMID: WOS:000274020200060; English.
- [61] Minakshi M, Mitchell DRG, Prince K. Incorporation of  $\text{TiB}_2$  additive into  $\text{MnO}_2$  cathode and its influence on rechargeability in an aqueous battery system. *Solid State Ionics*. 2008;179(9–10):355–361. PubMed PMID: WOS:000255992700008; English.
- [62] Raghuvver V, Manthiram A. Improved rechargeability of manganese oxide cathodes in alkaline cells in the presence of  $\text{TiB}_2$  and  $\text{TiS}_2$ . *J Power Sources*. 2006;159(2):1468–1473. PubMed PMID: WOS:000240959500089; English.
- [63] Raghuvver V, Manthiram A. Role of  $\text{TiB}_2$  and  $\text{Bi}_2\text{O}_3$  additives on the rechargeability of  $\text{MnO}_2$  in alkaline cells. *J Power Sources*. 2006;163(1):598–603. PubMed PMID: WOS:000244317100095; English.
- [64] Lee B, Yoon CS, Lee HR, et al. Electrochemically-induced reversible transition from the tunneled to layered polymorphs of manganese dioxide. *Sci Rep*. 2015;4:6066. DOI:10.1038/srep06066. <http://www.nature.com/srep/2014/140814/srep06066/abs/srep06066.html#supplementary-information>.
- [65] Lee B, Seo HR, Lee HR, et al. Critical role of pH evolution of electrolyte in the reaction mechanism for rechargeable zinc batteries. *ChemSusChem*. 2016;9(20):2948–2956. DOI:10.1002/cssc.201600702.
- [66] Zhi J, Li SK, Han M, et al. Unveiling conversion reaction on intercalation-based transition metal oxides for high power, high energy aqueous lithium battery. *Adv Energy Mater*. 2018;8(32):1802254. PubMed PMID: WOS:000450269900016; English.

- [67] Li Y, Wang SY, Salvador JR, et al. Reaction mechanisms for long-life rechargeable Zn/MnO<sub>2</sub> batteries. *Chem Mater.* 2019;31(6):2036–2047. PubMed PMID: WOS:000462950400023; English.
- [68] Tompsett DA, Parker SC, Bruce PG, et al. Nanostructuring of β-MnO<sub>2</sub>: the important role of surface to bulk ion migration. *Chem Mater.* 2013;25(4):536–541. PubMed PMID: WOS:000315618500004; English.
- [69] Tompsett DA, Islam MS. Surfaces of rutile MnO<sub>2</sub> are electronically conducting, whereas the bulk material is insulating. *J Phys Chem C.* 2014;118(43):25009–25015. PubMed PMID: WOS:000344135500024; English.
- [70] Cheng FY, Zhao JZ, Song W, et al. Facile controlled synthesis of MnO<sub>2</sub> nanostructures of novel shapes and their application in batteries. *Inorg Chem.* 2006;45(5):2038–2044. PubMed PMID: WOS:000235787300024; English.
- [71] Zhang K, Han XP, Hu Z, et al. Nanostructured Mn-based oxides for electrochemical energy storage and conversion. *Chem Soc Rev.* 2015;44(3):699–728. DOI:10.1039/c4cs00218k. PubMed PMID: ISI:000348922100007; English.
- [72] Etacheri V, Marom R, Elazari R, et al. Challenges in the development of advanced Li-ion batteries: a review. *Energy Environ Sci.* 2011;4(9):3243–3262. DOI:10.1039/c1ee01598b. PubMed PMID: ISI:000294306900010; English.
- [73] Tarascon JM, Armand M. Issues and challenges facing rechargeable lithium batteries. *Nature.* 2001;414(6861):359–367. DOI:10.1038/35104644. PubMed PMID: ISI:000172150700056; English.
- [74] Tarascon JM. Key challenges in future Li-battery research. *Philos Trans R Soc A Math Phys Eng Sci.* 2010;368(1923):3227–3241. DOI:10.1098/rsta.2010.0112. PubMed PMID: ISI:000278942500002; English.
- [75] Nishi Y. Lithium ion secondary batteries; past 10 years and the future. *J Power Sources.* 2001;100(1-2):101–106. DOI:10.1016/S0378-7753(01)00887-4. PubMed PMID: ISI:000172390700010; English.
- [76] Kim SW, Seo DH, Ma XH, et al. Electrode materials for rechargeable sodium-ion batteries: potential alternatives to current lithium-ion batteries. *Adv Energy Mater.* 2012;2(7):710–721. DOI:10.1002/aenm.201200026. PubMed PMID: ISI:000306311100002; English.
- [77] Augustyn V, Simon P, Dunn B. Pseudocapacitive oxide materials for high-rate electrochemical energy storage. *Energy Environ Sci.* 2014;7(5):1597–1614. DOI:10.1039/C3ee44164d. PubMed PMID: ISI:000335013700005; English.
- [78] Kotz R, Carlen M. Principles and applications of electrochemical capacitors. *Electrochim Acta.* 2000;45(15–16):2483–2498. DOI:10.1016/S0013-4686(00)00354-6. PubMed PMID: ISI:000087352000020; English.
- [79] Barrero R, Van Mierlo J, Tackoen X. Energy Savings in public transport. *IEEE Veh Technol Mag.* 2008;3(3):26–36. DOI:10.1109/Mvt.2008.927485. PubMed PMID: ISI:000207484500005; English.
- [80] Ribeiro PF, Johnson BK, Crow ML, et al. Energy storage systems for advanced power applications. *Proc IEEE.* 2001;89(12):1744–1756. DOI:10.1109/5.975900. PubMed PMID: ISI:000173303900003; English.
- [81] Trasatti S, Buzzanca G. Ruthenium dioxide: a new interesting electrode material. *Solid states structure and electrochemical behaviour.* *J Electroanal Chem.* 1971;29(2):A1–A5. DOI:10.1016/0368-1874(71)85100-6. PubMed PMID: ISI:A1971I585800025; English.
- [82] Cao JY, Li XH, Wang YM, et al. Materials and fabrication of electrode scaffolds for deposition of MnO<sub>2</sub> and their true performance in supercapacitors. *J Power Sources.* 2015;293:657–674. DOI:10.1016/j.jpowsour.2015.05.115. PubMed PMID: ISI:000358809700077; English.
- [83] Gummow RJ, de kock A, Thackeray MM. Improved capacity retention in rechargeable 4 V lithium/lithium-manganese oxide (spinel) cells. *Solid State Ionics.* 1994;69(1):59–67. DOI:10.1016/0167-2738(94)90450-2. PubMed PMID: ISI:A1994NW60600008; English.
- [84] Reddy RN, Reddy RG. Sol-gel MnO<sub>2</sub> as an electrode material for electrochemical capacitors. *J Power Sources.* 2003;124(1):330–337. DOI:10.1016/S0378-7753(03)00600-1. PubMed PMID: ISI:000185563800049; English.
- [85] Ohzuku T, Kitagawa M, Hirai T. Electrochemistry of manganese dioxide in lithium nonaqueous cell. *J Electrochem Soc.* 1990;137(3):769–775. DOI:10.1149/1.2086552. PubMed PMID: ISI:A1990CR91500005; English.
- [86] Park J, Lu W, Sastry AM. Numerical simulation of stress evolution in lithium manganese dioxide particles due to coupled phase transition and intercalation. *J Electrochem Soc.* 2011;158(2):A201–A206. DOI:10.1149/1.3526597. PubMed PMID: ISI:000285765600020; English.
- [87] Lee HY, Goodenough JB. Supercapacitor behavior with KCl electrolyte. *J Solid State Chem.* 1999;144(1):220–223. DOI:10.1006/jssc.1998.8128. PubMed PMID: ISI:000080288500031; English.
- [88] Qu QT, Zhang P, Wang B, et al. Electrochemical performance of MnO<sub>2</sub> nanorods in neutral aqueous electrolytes as a cathode for asymmetric supercapacitors. *J Phys Chem C.* 2009;113(31):14020–14027. DOI:10.1021/jp8113094. PubMed PMID: ISI:000268478700079; English.
- [89] Xu CJ, Kang FY, Li BH, et al. Recent progress on manganese dioxide based supercapacitors. *J Mater Res.* 2010;25(8):1421–1432. DOI:10.1557/Jmr.2010.0211. PubMed PMID: ISI:000280447400003; English.
- [90] Wei WF, Cui XW, Chen WX, et al. Manganese oxide-based materials as electrochemical supercapacitor electrodes. *Chem Soc Rev.* 2011;40(3):1697–1721. DOI:10.1039/c0cs00127a. PubMed PMID: ISI:000287585000031; English.
- [91] Arico AS, Bruce P, Scrosati B, et al. Nanostructured materials for advanced energy conversion and storage devices. *Nat Mater.* 2005;4(5):366–377. DOI:10.1038/nmat1368. PubMed PMID: ISI:000228834000008; English.
- [92] Yu A. *Electrochemical supercapacitors for energy storage and delivery: fundamentals and applications.* Boca Raton: Taylor & Francis; 2013. Green chemistry and chemical engineering.
- [93] Béguin F, Frackowiak E. *Supercapacitors: materials, systems, and applications.* Weinheim: Wiley-VCH; 2013. Materials for sustainable energy and development.
- [94] Frackowiak E. Carbon materials for supercapacitor application. *Phys Chem Chem Phys.* 2007;9(15):1774–1785. DOI:10.1039/b618139m. PubMed PMID: ISI:000245472600003; English.

- [95] Becker HI, inventor. Low voltage electrolytic capacitor patent 2,800,616. 1957.
- [96] Choi NS, Chen ZH, Freunberger SA, et al. Challenges facing lithium batteries and electrical double-layer capacitors. *Angew Chem, Int Ed.* 2012;51(40):9994–10024. DOI:10.1002/anie.201201429. PubMed PMID: ISI:000309181700007; English.
- [97] Simon P, Gogotsi Y, Dunn B. Where do batteries end and supercapacitors begin? *Science.* 2014;343(6176):1210–1211. DOI:10.1126/science.1249625. PubMed PMID: ISI:000332728500025; English.
- [98] Conway BE. *Electrochemical supercapacitors: scientific fundamentals and technological applications.* New York: Plenum Press; 1999.
- [99] Conway BE. Transition from “supercapacitor” to “battery” behavior in electrochemical energy storage. *J Electrochem Soc.* 1991;138(6):1539–1548. DOI:10.1149/1.2085829. PubMed PMID: ISI:A1991FQ10400005; English.
- [100] Brousse T, Belanger D, Long JW. To be or not to be pseudocapacitive? *J Electrochem Soc.* 2015;162(5):A5185–A5189. DOI:10.1149/2.0201505jes. PubMed PMID: ISI:000351976200026; English.
- [101] Conway BE, Birss V, Wojtowicz J. The role and utilization of pseudocapacitance for energy storage by supercapacitors. *J Power Sources.* 1997;66(1–2):1–14. DOI:10.1016/S0378-7753(96)02474-3. PubMed PMID: ISI:A1997XJ43700001; English.
- [102] Toupin M, Brousse T, Belanger D. Charge storage mechanism of MnO<sub>2</sub> electrode used in aqueous electrochemical capacitor. *Chem Mater.* 2004;16(16):3184–3190. DOI:10.1021/cm049649j. PubMed PMID: ISI:000223162700028; English.
- [103] Lee HY, Manivannan V, Goodenough JB. Electrochemical capacitors with KCl electrolyte. *Cr Acad Sci Li C.* 1999;2(11–13):565–577. DOI:10.1016/S1387-1609(00)88567-9. PubMed PMID: ISI:000084620300006; English.
- [104] Pang SC, Anderson MA, Chapman TW. Novel electrode materials for thin-film ultracapacitors: comparison of electrochemical properties of sol-gel-derived and electrodeposited manganese dioxide. *J Electrochem Soc.* 2000;147(2):444–450. DOI:10.1149/1.1393216. PubMed PMID: ISI:000085294400009; English.
- [105] Jones DJ, Wortham E, Roziere J, et al. Manganese oxide nanocomposites: preparation and some electrochemical properties. *J Phys Chem Solids.* 2004;65(2–3):235–239. DOI:10.1016/j.jpics.2003.10.020. PubMed PMID: ISI:000188884900025; English.
- [106] Nishimura K, Douzono T, Kasai M, et al. Spinel-type lithium-manganese oxide cathodes for rechargeable lithium batteries. *J Power Sources.* 1999;81–82:420–424. DOI:10.1016/S0378-7753(99)00224-4. PubMed PMID: ISI:000084090300078; English.
- [107] Hsieh YC, Lee KT, Lin YP, et al. Investigation on capacity fading of aqueous MnO<sub>2</sub>·nH<sub>2</sub>O electrochemical capacitor. *J Power Sources.* 2008;177(2):660–664. DOI:10.1016/j.jpowsour.2007.11.026. PubMed PMID: ISI:000253873700051; English.
- [108] Ataherian F, Lee KT, Wu NL. Long-term electrochemical behaviors of manganese oxide aqueous electrochemical capacitor under reducing potentials. *Electrochim Acta.* 2010;55(25):7429–7435. DOI:10.1016/j.electacta.2010.01.102. PubMed PMID: ISI:000282849100002; English.
- [109] Wang HQ, Yang GF, Li QY, et al. Porous nano-MnO<sub>2</sub>: large scale synthesis via a facile quick-redox procedure and application in a supercapacitor. *New J Chem.* 2011;35(2):469–475. DOI:10.1039/c0nj00712a. PubMed PMID: ISI:000286893300027; English.
- [110] Devaraj S, Munichandraiah N. Electrochemical supercapacitor studies of nanostructured α-MnO<sub>2</sub> synthesized by microemulsion method and the effect of annealing. *J Electrochem Soc.* 2007;154(2):A80–A88. DOI:10.1149/1.2404775. PubMed PMID: ISI:000243380200004; English.
- [111] Lee HY, Kim SW, Lee HY. Expansion of active site area and improvement of kinetic reversibility in electrochemical pseudocapacitor electrode. *Electrochem Solid-State Lett.* 2001;4(3):A19–A22. DOI:10.1149/1.1346536. PubMed PMID: ISI:000167326100001; English.
- [112] Lu XH, Zheng DZ, Zhai T, et al. Facile synthesis of large-area manganese oxide nanorod arrays as a high-performance electrochemical supercapacitor. *Energy Environ Sci.* 2011;4(8):2915–2921. DOI:10.1039/c1ee01338f. PubMed PMID: ISI:000293213600038; English.
- [113] Wang YT, Lu AH, Zhang HL, et al. Synthesis of nanostructured mesoporous manganese oxides with three-dimensional frameworks and their application in supercapacitors. *J Phys Chem C.* 2011;115(13):5413–5421. DOI:10.1021/jp110938x. PubMed PMID: ISI:000288885900029; English.
- [114] Yousefi T, Golikand AN, Mashhadizadeh MH, et al. Template-free synthesis of MnO<sub>2</sub> nanowires with secondary flower like structure: characterization and supercapacitor behavior studies. *Curr Appl Phys.* 2012;12(1):193–198. DOI:10.1016/j.cap.2011.05.038. PubMed PMID: ISI:000296525700037; English.
- [115] Wang XY, Wang XY, Huang WG, et al. Sol-gel template synthesis of highly ordered MnO<sub>2</sub> nanowire arrays. *J Power Sources.* 2005;140(1):211–215. DOI:10.1016/j.jpowsour.2004.07.033. PubMed PMID: ISI:000226265900025; English.
- [116] Zou RJ, Zhang ZY, Yuen MF, et al. Dendritic heterojunction nanowire arrays for high-performance supercapacitors. *Sci Rep.* 2015;5. DOI:10.1038/Srep07862. PubMed PMID: ISI:000347978600001; English.
- [117] Jiang RR, Huang T, Liu JL, et al. A novel method to prepare nanostructured manganese dioxide and its electrochemical properties as a supercapacitor electrode. *Electrochim Acta.* 2009;54(11):3047–3052. DOI:10.1016/j.electacta.2008.12.007. PubMed PMID: ISI:000265342100015; English.
- [118] Cai ZP, Zhou HB, Li WS, et al. Surface treatment method of cathodic current-collector and its effect on performances of batteries. *Rare Metal Mater Eng.* 2009;38(9):1676–1680. PubMed PMID: WOS:000276325200039; Chinese.
- [119] Athouel L, Moser F, Dugas R, et al. Variation of the MnO<sub>2</sub> birnessite structure upon charge/discharge in an electrochemical supercapacitor electrode in aqueous Na<sub>2</sub>SO<sub>4</sub> electrolyte. *J Phys Chem C.* 2008;112(18):7270–7277. DOI:10.1021/Jp0773029. PubMed PMID: ISI:000255486800024; English.
- [120] Subramanian V, Zhu HW, Wei BQ. Nanostructured MnO<sub>2</sub>: hydrothermal synthesis and electrochemical properties as a supercapacitor electrode material. *J Power Sources.* 2006;159(1):361–364. DOI:10.1016/j.

- jpowsour.2006.04.012. PubMed PMID: ISI:000241012000072; English.
- [121] Lei R, Zhang H, Fang Q, et al. MnO<sub>2</sub> nanowires electrodeposited on freestanding graphenated carbon nanotubes as binder-free electrodes with enhanced supercapacitor performance. *Mater Lett*. 2019;249:140–142. PubMed PMID: WOS:000467535500036; English.
- [122] Zhao Y, Dai MZ, Zhao DP, et al. Asymmetric pseudocapacitors based on dendrite-like MnO<sub>2</sub> nanostructures. *Crytengcomm*. 2019;21(21):3349–3355. PubMed PMID: WOS:000471020900011; English.
- [123] Zhu C, Yang L, Seo JK, et al. Self-branched  $\alpha$ -MnO<sub>2</sub>/ $\delta$ -MnO<sub>2</sub> heterojunction nanowires with enhanced pseudocapacitance. *Mater Horizons*. 2017. DOI:10.1039/c6mh00556j.
- [124] Kim JH, Lee KH, Overzet LJ, et al. Synthesis and electrochemical properties of spin-capable carbon nanotube sheet/MnOx composites for high-performance energy storage devices. *Nano Lett*. 2011;11(7):2611–2617. DOI:10.1021/nl200513a. PubMed PMID: ISI:000292849400007; English.
- [125] Li Q, Wang ZL, Li GR, et al. Design and synthesis of MnO<sub>2</sub>/Mn/MnO<sub>2</sub> Sandwich-structured nanotube arrays with high supercapacitive performance for electrochemical energy storage. *Nano Lett*. 2012;12(7):3803–3807. DOI:10.1021/nl301748m. PubMed PMID: ISI:000306296200075; English.
- [126] Zhao YQ, Zhao DD, Tang PY, et al. MnO<sub>2</sub>/graphene/nickel foam composite as high performance supercapacitor electrode via a facile electrochemical deposition strategy. *Mater Lett*. 2012;76:127–130. DOI:10.1016/j.matlet.2012.02.097. PubMed PMID: ISI:000303623000037; English.
- [127] Lei ZB, Zhang JT, Zhao XS. Ultrathin MnO<sub>2</sub> nanofibers grown on graphitic carbon spheres as high-performance asymmetric supercapacitor electrodes. *J Mater Chem*. 2012;22(1):153–160. DOI:10.1039/c1jm13872c. PubMed PMID: ISI:000297598400020; English.
- [128] Kang JL, Hirata A, Kang LJ, et al. Enhanced supercapacitor performance of MnO<sub>2</sub> by atomic doping. *Angew Chem Int Edit*. 2013;52(6):1664–1667. DOI:10.1002/anie.201208993. PubMed PMID: ISI:000314650600006; English.
- [129] Wang YH, Zhitomirsky I. Cathodic electrodeposition of Ag-doped manganese dioxide films for electrodes of electrochemical supercapacitors. *Mater Lett*. 2011;65(12):1759–1761. DOI:10.1016/j.matlet.2011.03.074. PubMed PMID: ISI:000291457200005; English.
- [130] Liu LH, Min M, Liu F, et al. Influence of vanadium doping on the supercapacitance performance of hexagonal birnessite. *J Power Sources*. 2015;277:26–35. DOI:10.1016/j.jpowsour.2014.12.004. PubMed PMID: ISI:000348957000004; English.
- [131] Ghodbane O, Pascal JL, Favier F. Microstructural effects on charge-storage properties in MnO<sub>2</sub>-based electrochemical supercapacitors. *ACS Appl Mater Inter*. 2009;1(5):1130–1139. DOI:10.1021/am900094e. PubMed PMID: ISI:000268665200022; English.
- [132] Brousse T, Toupin M, Dugas R, et al. Crystalline MnO<sub>2</sub> as possible alternatives to amorphous compounds in electrochemical supercapacitors. *J Electrochem Soc*. 2006;153(12):A2171–A2180. DOI:10.1149/1.2352197. PubMed PMID: ISI:000241757400001; English.
- [133] Li GR, Feng ZP, Ou YN, et al. Mesoporous MnO<sub>2</sub>/carbon Aerogel composites as promising electrode materials for high-performance supercapacitors. *Langmuir*. 2010;26(4):2209–2213. DOI:10.1021/la903947c. PubMed PMID: ISI:000274342200005; English.
- [134] Xu CJ, Wei CG, Li BH, et al. Charge storage mechanism of manganese dioxide for capacitor application: effect of the mild electrolytes containing alkaline and alkaline-earth metal cations. *J Power Sources*. 2011;196(18):7854–7859. DOI:10.1016/j.jpowsour.2011.04.052. PubMed PMID: ISI:000293939500071; English.
- [135] Xu CJ, Du HD, Li BH, et al. Asymmetric activated carbon-manganese dioxide capacitors in mild aqueous electrolytes containing alkaline-earth cations. *J Electrochem Soc*. 2009;156(6):A435–A441. DOI:10.1149/1.3106112. PubMed PMID: ISI:000265737600006; English.
- [136] Ghaemi M, Ataherian F, Zolfaghari A, et al. Charge storage mechanism of sonochemically prepared MnO<sub>2</sub> as supercapacitor electrode: effects of physi-sorbed water and proton conduction. *Electrochim Acta*. 2008;53(14):4607–4614. DOI:10.1016/j.electacta.2007.12.040. PubMed PMID: ISI:000255604900001; English.
- [137] Xu CJ, Du HD, Li BH, et al. Capacitive behavior and charge storage mechanism of manganese dioxide in aqueous solution containing bivalent cations. *J Electrochem Soc*. 2009;156(1):A73–A78. DOI:10.1149/1.3021013. PubMed PMID: ISI:000261209800014; English.
- [138] Ji CC, Xu MW, Bao SJ, et al. Effect of alkaline and alkaline-earth cations on the supercapacitor performance of MnO<sub>2</sub> with various crystallographic structures. *J Solid State Electrochem*. 2013;17(5):1357–1368. DOI:10.1007/s10008-013-2001-y. PubMed PMID: ISI:000320374300011; English.
- [139] Andreas H. Self-Discharge in electrochemical capacitors: a perspective article. *J Electrochem Soc*. 2015;162(5):A5047–A5053.
- [140] Kaus M, Kowal J, Sauer DU. Modelling the effects of charge redistribution during self-discharge of supercapacitors. *Electrochim Acta*. 2010;55(25):7516–7523. DOI:10.1016/j.electacta.2010.01.002. PubMed PMID: ISI:000282849100016; English.
- [141] Du Pasquier A, Plitz I, Menocal S, et al. A comparative study of Li-ion battery, supercapacitor and non-aqueous asymmetric hybrid devices for automotive applications. *J Power Sources*. 2003;115(1):171–178. DOI:10.1016/S0378-7753(02)00718-8. PubMed PMID: ISI:000182004800024; English.
- [142] Andreas HA, Black JM, Oickle AA. Self-discharge in manganese oxide electrochemical capacitor electrodes in aqueous electrolytes with comparisons to faradaic and charge redistribution models. *Electrochim Acta*. 2014;140:116–124. DOI:10.1016/j.electacta.2014.03.104. PubMed PMID: ISI:000342528600017; English.
- [143] Armand M, Tarascon JM. Building better batteries. *Nature*. 2008;451(7179):652–657. PubMed PMID: WOS:000252929500029; English.
- [144] Beck F, Ruetschi P. Rechargeable batteries with aqueous electrolytes. *Electrochim Acta*. 2000;45(15–16):2467–2482. DOI:10.1016/S0013-4686(00)00344-3. PubMed PMID: ISI:000087352000019; English.
- [145] Luo JY, Xia YY. Aqueous lithium-ion battery LiTi<sub>2</sub>(PO<sub>4</sub>)<sub>3</sub>/LiMn<sub>2</sub>O<sub>4</sub> with high power and energy densities as well as superior cycling stability. *Adv*

- Funct Mater. 2007;17(18):3877–3884. DOI:10.1002/adfm.200700638. PubMed PMID: ISI:000251831000024; English.
- [146] Rana J, Stan M, Kloepsch R, et al. Structural changes in  $\text{Li}_2\text{MnO}_3$  cathode material for Li-ion batteries. *Adv Energy Mater.* 2014;4(5). DOI:10.1002/Aenm.201300998. PubMed PMID: ISI:000333708100016; English.
- [147] Cachet-Vivier C, Bach S, Pereira-Ramos JP. Electrochemical proton insertion in manganese spinel oxides from aqueous borate solution. *Electrochim Acta.* 1999;44(16):2705–2709. DOI:10.1016/S0013-4686(98)00377-6. PubMed PMID: ISI:000079318400004; English.
- [148] Choi J, Alvarez E, Arunkumar TA, et al. Proton insertion into oxide cathodes during chemical delithiation. *Electrochem Solid State Lett.* 2006;9(5):A241–A244. DOI:10.1149/1.2184495. PubMed PMID: ISI:000236228900006; English.
- [149] Li W, Mckinnon WR, Dahn JR. Lithium intercalation from aqueous-solutions. *J Electrochem Soc.* 1994;141(9):2310–2316. DOI:10.1149/1.2055118. PubMed PMID: ISI:A1994PG28600022; English.
- [150] Hunter JC. Preparation of a new crystal form of manganese dioxide:  $\lambda\text{-MnO}_2$ . *J Solid State Chem.* 1981;39(2):142–147. DOI:10.1016/0022-4596(81)90323-6. PubMed PMID: ISI:A1981MG83700002; English.
- [151] Alias N, Mohamad AA. Advances of aqueous rechargeable lithium-ion battery: a review. *J Power Sources.* 2015;274:237–251. DOI:10.1016/j.jpowsour.2014.10.009. PubMed PMID: ISI:000347268700030; English.
- [152] Shao-Horn Y, Hackney SA, Kahaian AJ, et al. Structural fatigue in spinel electrodes in Li/Li-x[Mn-2]O-4 cells. *J Power Sources.* 1999;81-82:496–499. DOI:10.1016/S0378-7753(98)00223-7. PubMed PMID: ISI:000084090300092; English.
- [153] Goodenough JB. Theory of the role of covalence in the perovskite-type manganites  $[\text{La},\text{M}(\text{II})]\text{MnO}_3$ . *Phys Rev.* 1955;100(2):564–573. DOI:10.1103/PhysRev.100.564. PubMed PMID: ISI:A1955WB70900016; English.
- [154] Binder L, Kordesch K, Urdl P. Improvements of the rechargeable alkaline  $\text{MnO}[\text{sub } 2\text{]}-\text{Zn}$  cell. *J Electrochem Soc.* 1996;143(1):13–17. DOI:10.1149/1.1836380.
- [155] Donne SW, Lawrance GA, Swinkels DAJ. Redox processes at the manganese dioxide electrode. *J Electrochem Soc.* 1997;144(9):2954–2961. DOI:10.1149/1.1837943.
- [156] Jang DH, Shin YJ, Oh SM. Dissolution of spinel oxides and capacity losses in 4 V  $\text{Li}/\text{Li}_x\text{Mn}_2\text{O}_4$  cells. *J Electrochem Soc.* 1996;143(7):2204–2211. DOI:10.1149/1.1836981. PubMed PMID: ISI:A1996UY44500030; English.
- [157] Xia YY, Yoshio M. An investigation of lithium ion insertion into spinel structure Li-Mn-O compounds. *J Electrochem Soc.* 1996;143(3):825–833. DOI:10.1149/1.1836544. PubMed PMID: ISI:A1996UC20300017; English.
- [158] Cui YL, Yuan Z, Bao WJ, et al. Investigation of lithium ion kinetics through  $\text{LiMn}_2\text{O}_4$  electrode in aqueous  $\text{Li}_2\text{SO}_4$  electrolyte. *J Appl Electrochem.* 2012;42(10):883–891. DOI:10.1007/s10800-012-0464-7. PubMed PMID: ISI:000309590800009; English.
- [159] Zhao MS, Huang GL, Zhang B, et al. Characteristics and electrochemical performance of  $\text{LiFe}_0.5\text{Mn}_0.5\text{PO}_4/\text{C}$  used as cathode for aqueous rechargeable lithium battery. *J Power Sources.* 2012;211:202–207. DOI:10.1016/j.jpowsour.2012.03.049. PubMed PMID: ISI:000305364900031; English.
- [160] Liu L, Tian FH, Wang XY, et al. Electrochemical behavior of spherical  $\text{LiNi}_1/3\text{Co}_1/3\text{Mn}_1/3\text{O}_2$  as cathode material for aqueous rechargeable lithium batteries. *J Solid State Electr.* 2012;16(2):491–497. DOI:10.1007/s10008-011-1357-0. PubMed PMID: ISI:000301040900011; English.
- [161] Li NC, Patrissi CJ, Che GL, et al. Rate capabilities of nanostructured  $\text{LiMn}_2\text{O}_4$  electrodes in aqueous electrolyte. *J Electrochem Soc.* 2000;147(6):2044–2049. DOI:10.1149/1.1393483. PubMed PMID: ISI:000087561800007; English.
- [162] Eftekhari A. Electrochemical behavior of thin-film  $\text{LiMn}_2\text{O}_4$  electrode in aqueous media. *Electrochim Acta.* 2001;47(3):495–499. DOI:10.1016/S0013-4686(01)00774-5. PubMed PMID: ISI:000172358600013; English.
- [163] Tonti D, Torralvo MJ, Enciso E, et al. Three-dimensionally ordered macroporous lithium manganese oxide for rechargeable lithium batteries. *Chem Mater.* 2008;20(14):4783–4790. DOI:10.1021/Cm702134s. PubMed PMID: ISI:000257666300036; English.
- [164] Tian L, Yuan AB. Electrochemical performance of nanostructured spinel  $\text{LiMn}_2\text{O}_4$  in different aqueous electrolytes. *J Power Sources.* 2009;192(2):693–697. DOI:10.1016/j.jpowsour.2009.03.002. PubMed PMID: ISI:000267270000063; English.
- [165] Tang W, Tian S, Liu LL, et al. Nanochain  $\text{LiMn}_2\text{O}_4$  as ultra-fast cathode material for aqueous rechargeable lithium batteries. *Electrochem Commun.* 2011;13(2):205–208. DOI:10.1016/j.elecom.2010.12.015. PubMed PMID: ISI:000287617700027; English.
- [166] Tang W, Liu LL, Tian S, et al.  $\text{LiMn}_2\text{O}_4$  nanorods as a super-fast cathode material for aqueous rechargeable lithium batteries. *Electrochem Commun.* 2011;13(11):1159–1162. DOI:10.1016/j.elecom.2011.09.008. PubMed PMID: ISI:000297492800003; English.
- [167] Zhao H, Chen DF, Yan M, et al. A novel two-step preparation of spinel  $\text{LiMn}_2\text{O}_4$  nanowires and its electrochemical performance characterization. *J Mater Res.* 2012;27(13):1750–1754. DOI:10.1557/jmr.2012.152. PubMed PMID: ISI:000307187900011; English.
- [168] Sinha NN, Munichandraiah N. Electrochemical conversion of  $\text{LiMn}_2\text{O}_4$  to  $\text{MgMn}_2\text{O}_4$  in aqueous electrolytes. *Electrochem Solid-State Lett.* 2008;11(11):F23–F26. DOI:10.1149/1.2972990. PubMed PMID: ISI:000259188600016; English.
- [169] Minakshi M. Looking beyond lithium-ion technology – aqueous NaOH battery. *Mater Sci Eng B.* 2012;177(20):1788–1792. PubMed PMID: WOS:000311926900011; English.
- [170] Chen L, Gu QW, Zhou XF, et al. New-concept batteries based on aqueous  $\text{Li}^+/\text{Na}^+$  mixed-ion electrolytes. *Sci Rep-UK.* 2013;3:1946. PubMed PMID: WOS:000319899500008; English.
- [171] Yuan CL, Zhang Y, Pan Y, et al. Investigation of the intercalation of polyvalent cations ( $\text{Mg}^{2+}$ ,  $\text{Zn}^{2+}$ ) into  $\lambda\text{-MnO}_2$  for rechargeable aqueous battery. *Electrochim Acta.* 2014;116:404–412. DOI:10.1016/j.electacta.2013.11.090. PubMed PMID: ISI:000331494400055; English.

- [172] Zhao MS, Zheng QY, Wang F, et al. Electrochemical performance of high specific capacity of lithium-ion cell  $\text{LiV}_3\text{O}_8/\text{LiMn}_2\text{O}_4$  with  $\text{LiNO}_3$  aqueous solution electrolyte. *Electrochim Acta*. 2011;56(11):3781–3784. PubMed PMID: WOS:000290692700005; English.
- [173] Stojadinovic J, Dushina A, Trocoli R, et al. Electrochemical characterization of gel electrolytes for aqueous lithium-ion batteries. *Chempluschem*. 2014;79(10):1507–1511. DOI:10.1002/cplu.201402143. PubMed PMID: ISI:000342797000013; English.
- [174] Abou-El-Sherbini KS, Askar MH. Lithium insertion into manganese dioxide polymorphs in aqueous electrolytes. *J Solid State Electr*. 2003;7(7):435–441. DOI:10.1007/s10008-002-0339-7. PubMed PMID: ISI:000184060300004; English.
- [175] Liu S, Pan GL, Yan NF, et al. Aqueous  $\text{TiO}_2/\text{Ni}(\text{OH})_2$  rechargeable battery with a high voltage based on proton and lithium insertion/extraction reactions. *Energ Environ Sci*. 2010;3(11):1732–1735. PubMed PMID: WOS:000283602400011; English.
- [176] Liu S, Ye SH, Li CZ, et al. Rechargeable aqueous lithium-ion battery of  $\text{TiO}_2/\text{LiMn}_2\text{O}_4$  with a high voltage. *J Electrochem Soc*. 2011;158(12):A1490–A1497. DOI:10.1149/2.094112jes. PubMed PMID: ISI:000297979300035; English.
- [177] Zhao MS, Song XP, Wang F, et al. Electrochemical performance of single crystalline spinel  $\text{LiMn}_2\text{O}_4$  nanowires in an aqueous  $\text{LiNO}_3$  solution. *Electrochim Acta*. 2011;56(16):5673–5678. DOI:10.1016/j.electacta.2011.04.025. PubMed PMID: ISI:000292428000032; English.
- [178] Zhao MS, Zhang B, Huang GL, et al. Electrochemical performance of modified  $\text{LiMn}_2\text{O}_4$  used as cathode material for an aqueous rechargeable lithium battery. *Energ Fuel*. 2012;26(2):1214–1219. DOI:10.1021/Ef201531t. PubMed PMID: ISI:000300275100048; English.
- [179] Ouatani LE, Dedryvere R, Siret C, et al. The effect of vinylene carbonate additive on surface film formation on both electrodes in Li-Ion batteries. *J Electrochem Soc*. 2009;156(2):A103–A113. DOI:10.1149/1.3029674. PubMed PMID: ISI:000261973600005; English.
- [180] Ushirogata K, Sodeyama K, Okuno Y, et al. Additive effect on reductive decomposition and binding of carbonate-based solvent toward solid electrolyte interphase formation in lithium-ion battery. *J Am Chem Soc*. 2013;135(32):11967–11974. DOI:10.1021/ja405079s. PubMed PMID: ISI:000323241200050; English.
- [181] Stojkovic IB, Cvjeticanin ND, Mentus SV. The improvement of the Li-ion insertion behaviour of  $\text{Li}_{1.05}\text{Cr}_{0.10}\text{Mn}_{1.85}\text{O}_4$  in an aqueous medium upon addition of vinylene carbonate. *Electrochem Commun*. 2010;12(3):371–373. DOI:10.1016/j.elecom.2009.12.037. PubMed PMID: ISI:000275784600011; English.
- [182] Kohler J, Makihara H, Uegaito H, et al.  $\text{LiV}_3\text{O}_8$ : characterization as anode material for an aqueous rechargeable Li-ion battery system. *Electrochim Acta*. 2000;46(1):59–65. DOI:10.1016/S0013-4686(00)00515-6. PubMed PMID: ISI:000165084300008; English.
- [183] Wang XJ, Hou YY, Zhu YS, et al. An aqueous rechargeable lithium battery using coated Li metal as anode. *Sci Rep-UK*. 2013;3. DOI:10.1038/Srep01401. PubMed PMID: ISI:000315720800003; English.
- [184] Nam KW, Kim S, Lee S, et al. The high performance of crystal water containing manganese birnessite cathodes for magnesium batteries. *Nano Lett*. 2015;15(6):4071–4079. PubMed PMID: WOS:000356316900063; English.
- [185] Alfaruqi MH, Islam S, Putro DY, et al. Structural transformation and electrochemical study of layered  $\text{MnO}_2$  in rechargeable aqueous zinc-ion battery. *Electrochim Acta*. 2018;276:1–11. PubMed PMID: WOS:000433042500001; English.
- [186] Sahadeo E, Song J, Gaskell K, et al. Investigation of the water-stimulated  $\text{Mg}_{2+}$  insertion mechanism in an electrodeposited  $\text{MnO}_2$  cathode using X-ray photoelectron spectroscopy. *Phys Chem Chem Phys*. 2018;20(4):2517–2526. PubMed PMID: WOS:000423505500039; English.
- [187] Liu Y, Qiao Y, Zhang WX, et al. Nanostructured alkali cation incorporated  $\delta\text{-MnO}_2$  cathode materials for aqueous sodium-ion batteries. *J Mater Chem A*. 2015;3(15):7780–7785. PubMed PMID: WOS:000352441100015; English.
- [188] Zhan P, Wang S, Yuan Y, et al. Facile synthesis of nanorod-like single crystalline  $\text{Na}_{0.44}\text{MnO}_2$  for high performance sodium-ion batteries. *J Electrochem Soc*. 2015;162(6):A1028–A1032. PubMed PMID: WOS:000353009300033; English.
- [189] Bai SL, Song JL, Wen YH, et al. Effects of zinc and manganese ions in aqueous electrolytes on structure and electrochemical performance of  $\text{Na}_{0.44}\text{MnO}_2$  cathode material. *RSC Adv*. 2016;6(47):40793–40798. PubMed PMID: WOS:000375270600021; English.
- [190] Shan XQ, Guo FH, Xu WQ, et al. High purity  $\text{Mn}_5\text{O}_8$  nanoparticles with a high overpotential to gas evolution reactions for high voltage aqueous sodium-ion electrochemical storage. *Front Energy*. 2017;11(3):383–400. PubMed PMID: WOS:000410770500015; English.
- [191] Tekin B, Sevinc S, Morcrette M, et al. A new sodium-based aqueous rechargeable battery system: the special case of  $\text{Na}_{0.44}\text{MnO}_2/\text{dissolved sodium polysulfide}$ . *Energy Technol-Ger*. 2017;5(12):2182–2188. PubMed PMID: WOS:000417757000007; English.
- [192] Yuan TC, Zhang JX, Pu XJ, et al. Novel alkaline  $\text{Zn}/\text{Na}_{0.44}\text{MnO}_2$  dual-ion battery with a high capacity and long cycle lifespan. *ACS Appl Mater Interfaces*. 2018;10(40):34108–34115. PubMed PMID: WOS:000447355300036; English.
- [193] Whitacre JF, Tevar A, Sharma S.  $\text{Na}_4\text{Mn}_9\text{O}_{18}$  as a positive electrode material for an aqueous electrolyte sodium-ion energy storage device. *Electrochem Commun*. 2010;12(3):463–466. PubMed PMID: WOS:000275784600034; English.
- [194] Il Park S, Gocheva I, Okada S, et al. Electrochemical properties of  $\text{NaTi}_2(\text{PO}_4)_3$  anode for rechargeable aqueous sodium-ion batteries. *J Electrochem Soc*. 2011;158(10):A1067–A1070. PubMed PMID: WOS:000294063000001; English.
- [195] Li Z, Young D, Xiang K, et al. Towards high power high energy aqueous sodium-ion batteries: the  $\text{NaTi}_2(\text{PO}_4)_3/\text{Na}_{0.44}\text{MnO}_2$  system. *Adv Energy Mater*. 2013;3(3):290–294. PubMed PMID: WOS:000316117800004; English.
- [196] Xu MW, Niu YB, Chen CJ, et al. Synthesis and application of ultra-long  $\text{Na}_{0.44}\text{MnO}_2$  submicron slabs as a

- cathode material for Na-ion batteries. *RSC Adv.* **2014**;4(72):38140–38143. PubMed PMID: WOS:000341455200026; English.
- [197] Shan XQ, Charles DS, Xu WQ, et al. Biphasic cobalt-manganese oxide with high capacity and rate performance for aqueous sodium-ion electrochemical energy storage. *Adv Funct Mater.* **2018**;28(3):1703266. PubMed PMID: WOS:000419866000001; English.
- [198] Boyd S, Dhall R, LeBeau JM, et al. Charge storage mechanism and degradation of P2-type sodium transition metal oxides in aqueous electrolytes. *J Mater Chem A.* **2018**;6(44):22266–22276. PubMed PMID: WOS:000456724800059; English.
- [199] Sauvage F, Laffont L, Tarascon JM, et al. Study of the insertion/deinsertion mechanism of sodium into  $\text{Na}_{0.44}\text{MnO}_2$ . *Inorg Chem.* **2007**;46(8):3289–3294. PubMed PMID: WOS:000245510200044; English.
- [200] Cao YL, Xiao LF, Wang W, et al. Reversible sodium ion insertion in single crystalline manganese oxide nanowires with long cycle life. *Adv Mater.* **2011**;23(28):3155–3315. PubMed PMID: WOS:000294091700007; English.
- [201] Kim DJ, Ponraj R, Kannan AG, et al. Diffusion behavior of sodium ions in  $\text{Na}_{0.44}\text{MnO}_2$  in aqueous and non-aqueous electrolytes. *J Power Sources.* **2013**;244:758–763. PubMed PMID: WOS:000324511600122; English.
- [202] Srimuk P, Lee J, Budak O, et al. In situ tracking of partial sodium desolvation of materials with capacitive, pseudocapacitive, and battery-like charge/discharge behavior in aqueous electrolytes. *Langmuir.* **2018**;34(44):13132–13143. PubMed PMID: WOS:000449722400006; English.
- [203] Jiang YL, Tan SS, Wei QL, et al. Pseudocapacitive layered birnessite sodium manganese dioxide for high-rate non-aqueous sodium ion capacitors. *J Mater Chem A.* **2018**;6(26):12259–12266. PubMed PMID: WOS:000437469300006; English.
- [204] Karikalan N, Karuppiah C, Chen SM, et al. Three-dimensional fibrous network of  $\text{Na}_{0.21}\text{MnO}_2$  for aqueous sodium-ion hybrid supercapacitors. *Chem A Eur J.* **2017**;23(10):2379–2386. PubMed PMID: WOS:000395583200021; English.
- [205] Hou Y, Tang HW, Li B, et al. Hexagonal-layered  $\text{Na}_{0.7}\text{MnO}_{2.05}$  via solvothermal synthesis as an electrode material for aqueous Na-ion supercapacitors. *Mater Chem Phys.* **2016**;171:137–144. PubMed PMID: WOS:000384703500020; English.
- [206] Ma H, Li CS, Su Y, et al. Studies on the vapour-transport synthesis and electrochemical properties of zinc micro-, meso- and nanoscale structures. *J Mater Chem.* **2007**;17(7):684–691. PubMed PMID: WOS:000244085100015; English.
- [207] Li Q, Xu P, Zhang B, et al. One-step synthesis of  $\text{Mn}_3\text{O}_4$ /reduced graphene oxide nanocomposites for oxygen reduction in nonaqueous Li-O-2 batteries. *Chem Commun.* **2013**;49(92):10838–10840. DOI:10.1039/c3cc46441e. PubMed PMID: WOS:000326219500022; English.
- [208] Toussaint G, Stevens P, Akrouf L, et al. Development of a rechargeable zinc-air battery. *Ecs Transactions.* **2010**;28(32):25–34. DOI:10.1149/1.3506338. PubMed PMID: WOS:000313571500003; English.
- [209] Lee JS, Kim ST, Cao R, et al. Metal-air batteries with high energy density: Li-air versus Zn-air. *Adv Energy Mater.* **2011**;1(1):34–50. PubMed PMID: WOS:000291725000003; English.
- [210] Trasatti S. Electrocatalysis by oxides — attempt at a unifying approach. *J Electroanal Chem Interfacial Electrochem.* **1980**;111(1):125–131. DOI:10.1016/S0022-0728(80)80084-2. PubMed PMID: ISI: A1980KF59400013; English.
- [211] Bikkarolla SK, Yu FJ, Zhou WZ, et al. A three-dimensional  $\text{Mn}_3\text{O}_4$  network supported on a nitrogenated graphene electrocatalyst for efficient oxygen reduction reaction in alkaline media. *J Mater Chem A.* **2014**;2(35):14493–14501. PubMed PMID: WOS:000340768000023; English.
- [212] Norskov JK, Rossmeisl J, Logadottir A, et al. Origin of the overpotential for oxygen reduction at a fuel-cell cathode. *J Phys Chem B.* **2004**;108(46):17886–17892. DOI:10.1021/jp047349j. PubMed PMID: WOS:000225079300029; English.
- [213] Quaino P, Juarez F, Santos E, et al. Volcano plots in hydrogen electrocatalysis – uses and abuses. *Beilstein J Nanotech.* **2014**;5:846–854. DOI:10.3762/bjnano.5.96. PubMed PMID: WOS:000337811200001; English.
- [214] Suntivich J, May KJ, Gasteiger HA, et al. A perovskite oxide optimized for oxygen evolution catalysis from molecular orbital principles. *Science.* **2011**;334(6061):1383–1385. PubMed PMID: WOS:000297787700047; English.
- [215] Hamdani M, Singh RN, Chartier P.  $\text{CO}_3\text{O}_4$  and Co-based spinel oxides bifunctional oxygen electrodes. *Int J Electrochem Sc.* **2010**;5(4):556–577. PubMed PMID: WOS:000278336100011; English.
- [216] Nikolova V, Iliev P, Petrov K, et al. Electrocatalysts and electrode design for bifunctional oxygen/air electrodes. *Nato Sci Peace Security Ser.* **2008**; 305–310. DOI:10.1007/978-1-4020-8903-9\_22. PubMed PMID: WOS:000260438200022; English.
- [217] Landon J, Demeter E, Inoglu N, et al. Spectroscopic characterization of mixed Fe-Ni oxide electrocatalysts for the oxygen evolution reaction in alkaline electrolytes. *ACS Catal.* **2012**;2(8):1793–1801. DOI:10.1021/cs3002644. PubMed PMID: WOS:000307257800031; English.
- [218] Mao L, Sotomura T, Nakatsu K, et al. Electrochemical characterization of catalytic activities of manganese oxides to oxygen reduction in alkaline aqueous solution. *J Electrochem Soc.* **2002**;149(4):A504–A507.
- [219] Cheng FY, Shen J, Ji WQ, et al. Selective synthesis of manganese oxide nanostructures for electrocatalytic oxygen reduction. *ACS Appl Mater Interfaces.* **2009**;1(2):460–466. PubMed PMID: WOS:000267535700035; English.
- [220] Zoltowski P, Drazic DM, Vorkapic L. Carbon air electrode with regenerative short time overload capacity. II. Effects of duroquinone and 2-amino-1,4 naphthoquinone. *J Appl Electrochem.* **1975**;5(1):79–87. DOI:10.1007/Bf00625962. PubMed PMID: WOS: A1975V981300008; English.
- [221] Crompton TR. Battery reference book. 3rd ed. London: Reed Educational and Professional Publishing; **2000**.
- [222] Cooper J. Powering future vehicles with the refueable zinc air battery. *Sci Technol Rev.* **1995**;10:6–13.
- [223] Wang ZH, Lin SS, Wang DM, et al. Anti-epidermal growth factor receptor tyrosine kinase activities of

- traditional Chinese medicine for cancer treatment. *Eur J Integr Med.* **2014**;6(5):565–570. DOI:10.1016/j.eujim.2014.05.006. PubMed PMID: ISI:000343923800009; English.
- [224] Cheng FY, Chen J. Metal-air batteries: from oxygen reduction electrochemistry to cathode catalysts. *Chem Soc Rev.* **2012**;41(6):2172–2192. PubMed PMID: WOS:000300797700012; English.
- [225] Jorissen L. Bifunctional oxygen/air electrodes. *J Power Sources.* **2006**;155(1):23–32. PubMed PMID: WOS:000236957800004; English.
- [226] Zhang P, Chen XF, Lian JS, et al. Structural selectivity of CO oxidation on Fe/N/C catalysts. *J Phys Chem C.* **2012**;116(33):17572–17579. DOI:10.1021/jp304097m. PubMed PMID: WOS:000307748700032; English.
- [227] Slominski AT, Kim TK, Shehabi HZ, et al. In vivo production of novel vitamin D2 hydroxy-derivatives by human placentas, epidermal keratinocytes, Caco-2 colon cells and the adrenal gland. *Mol Cell Endocrinol.* **2014**;383(1-2):181–192. DOI:10.1016/j.mce.2013.12.012. PubMed PMID: ISI:000332049400019; English.
- [228] Rasiyah P, Tseung ACC. The role of the lower metal oxide/higher metal oxide couple in oxygen evolution reactions. *J Electrochem Soc.* **1984**;131(4):803–808. DOI:10.1149/1.2115703. PubMed PMID: WOS:A1984SL25600021; English.
- [229] Gorlin Y, Jaramillo TF. A bifunctional nonprecious metal catalyst for oxygen reduction and water oxidation. *J Am Chem Soc.* **2010**;132(39):13612–13614. DOI:10.1021/ja104587v. PubMed PMID: WOS:000282864100017; English.
- [230] Casas-Cabanas M, Binotto G, Larcher D, et al. Defect chemistry and catalytic activity of nanosized CO<sub>3</sub>O<sub>4</sub>. *Chem Mater.* **2009**;21(9):1939–1947. PubMed PMID: WOS:000265781000028; English.
- [231] Ding YS, Shen XF, Sithambaram S, et al. Synthesis and catalytic activity of cryptomelane-type manganese dioxide nanomaterials produced by a novel solvent-free method. *Chem Mater.* **2005**;17(21):5382–5389. DOI:10.1021/cm051294w. PubMed PMID: WOS:000232743700025; English.
- [232] Benbow EM, Kelly SP, Zhao L, et al. Oxygen reduction properties of bifunctional  $\alpha$ -manganese oxide electrocatalysts in aqueous and organic electrolytes. *J Phys Chem C.* **2011**;115(44):22009–22017. PubMed PMID: WOS:000296394300059; English.
- [233] Cao YL, Yang HX, Ai XP, et al. The mechanism of oxygen reduction on MnO<sub>2</sub>-catalyzed air cathode in alkaline solution. *J Electroanal Chem.* **2003**;557:127–134. PubMed PMID: WOS:000186239000012; English.
- [234] Zhou M, Zhang X, Wei JM, et al. Morphology-controlled synthesis and novel microwave absorption properties of hollow urchinlike  $\alpha$ -MnO<sub>2</sub> nanostructures. *J Phys Chem C.* **2011**;115(5):1398–1402. DOI:10.1021/jp106652x. PubMed PMID: WOS:000286868600004; English.
- [235] Zheng YP, Song K, Jung J, et al. Critical descriptor for the rational design of oxide-based catalysts in rechargeable Li-O<sub>2</sub> batteries: surface oxygen density. *Chem Mater.* **2015**;27(9):3243–3249. DOI:10.1021/acs.chemmater.5b00056. PubMed PMID: ISI:000354578600012; English.
- [236] Sehlakumar K, Kumar SMS, Thangamuthu R, et al. Development of shape-engineered  $\alpha$ -MnO<sub>2</sub> materials as bi-functional catalysts for oxygen evolution reaction and oxygen reduction reaction in alkaline medium. *Int J Hydrogen Energy.* **2014**;39(36):21024–21036. DOI:10.1016/j.ijhydene.2014.10.088. PubMed PMID: ISI:000347576200017; English.
- [237] Oxford GAE, Chaka AM. Structure and stability of hydrated  $\beta$ -MnO<sub>2</sub> surfaces. *J Phys Chem C.* **2012**;116(21):11589–11605. DOI:10.1021/jp302268m. PubMed PMID: WOS:000304574500020; English.
- [238] Lindan PJD, Zhang CJ. Exothermic water dissociation on the rutile TiO<sub>2</sub>(110) surface. *Phys Rev B.* **2005**;72(7). DOI:10.1103/Physrevb.72.075439. PubMed PMID: WOS:000231564500192; English.
- [239] Feng J, Liang YY, Wang HL, et al. Engineering manganese oxide/nanocarbon hybrid materials for oxygen reduction electrocatalysis. *Nano Res.* **2012**;5(10):718–725. DOI:10.1007/s12274-012-0256-8. PubMed PMID: WOS:000310087400006; English.
- [240] N. Koshiba HH, K. Momose, A. Ohta. US Patent 4,595,643. 1984.
- [241] Roche I, Chainet E, Chatenet M, et al. Carbon-supported manganese oxide nanoparticles as electrocatalysts for the oxygen reduction reaction (ORR) in alkaline medium: physical characterizations and ORR mechanism. *J Phys Chem C.* **2007**;111(3):1434–1443. DOI:10.1021/jp0647986. PubMed PMID: ISI:000245005400058; English.
- [242] Zhang JT, Guo CX, Zhang LY, et al. Direct growth of flower-like manganese oxide on reduced graphene oxide towards efficient oxygen reduction reaction. *Chem Commun.* **2013**;49(56):6334–6336. DOI:10.1039/c3cc42127a. PubMed PMID: WOS:000320555800028; English.
- [243] Gorlin Y, Chung CJ, Nordlund D, et al. Mn<sub>3</sub>O<sub>4</sub> supported on glassy carbon: an active non-precious metal catalyst for the oxygen reduction reaction. *ACS Catal.* **2012**;2(12):2687–2694. PubMed PMID: WOS:000312170100030; English.
- [244] Wang XY, Sebastian PJ, Smit MA, et al. Studies on the oxygen reduction catalyst for zinc-air battery electrode. *J Power Sources.* **2003**;124(1):278–284. DOI:10.1016/S0378-7753(03)00737-7. PubMed PMID: WOS:000185563800041; English.
- [245] Neburchilov V, Wang HJ, Martin JJ, et al. A review on air cathodes for zinc-air fuel cells. *J Power Sources.* **2010**;195(5):1271–1291. PubMed PMID: WOS:000272058600001; English.
- [246] Wang JF, Li HR, Xu NN, et al. Optimization of rechargeable zinc-air battery with CO<sub>3</sub>O<sub>4</sub>/MnO<sub>2</sub>/CNT bifunctional catalyst: effects of catalyst loading, binder content, and spraying area. *Ionics (Kiel).* **2018**;24(12):3877–3884. PubMed PMID: WOS:000450111000016; English.
- [247] Li XM, Dong F, Xu NN, et al. CO<sub>3</sub>O<sub>4</sub>/MnO<sub>2</sub>/hierarchically porous carbon as superior bifunctional electrodes for liquid and all-solid-state rechargeable zinc-air batteries. *ACS Appl Mater Interfaces.* **2018**;10(18):15591–15601. PubMed PMID: WOS:000432205800030; English.
- [248] Du G, Liu X, Zong Y, et al. CO<sub>3</sub>O<sub>4</sub> nanoparticle-modified MnO<sub>2</sub> nanotube bifunctional oxygen cathode catalysts for rechargeable zinc-air batteries. *Nanoscale.* **2013**;5(11):4657–4661.
- [249] Cheng FY, Shen JA, Peng B, et al. Rapid room-temperature synthesis of nanocrystalline spinels as oxygen reduction and evolution electrocatalysts. *Nat Chem.* **2011**;3(1):79–84. PubMed PMID: WOS:000285336900021; English.

- [250] Ni SL, Zhang HJ, Zhao YH, et al. Single atomic Ag enhances the bifunctional activity and cycling stability of MnO<sub>2</sub>. *Chem Eng J.* **2019**;366:631–638. PubMed PMID: WOS:000459903100061; English.
- [251] Mathur A, Halder A. One-step synthesis of bifunctional iron-doped manganese oxide nanorods for rechargeable zinc-air batteries. *Catal Sci Technol.* **2019**;9(5):1245–1254. PubMed PMID: WOS:000460322700015; English.
- [252] Wu QM, Jiang LH, Qi LT, et al. Electrocatalytic performance of Ni modified MnOX/C composites toward oxygen reduction reaction and their application in Zn-air battery. *Int J Hydrogen Energy.* **2014**;39(7):3423–3432. PubMed PMID: WOS:000331917400039; English.
- [253] Lee JH, Black R, Popov G, et al. The role of vacancies and defects in Na<sub>0.44</sub>MnO<sub>2</sub> nanowire catalysts for lithium-oxygen batteries. *Energy Environ Sci.* **2012**;5(11):9558–9565. DOI:10.1039/c2ee21543h. PubMed PMID: WOS:000310006200041; English.
- [254] Tseng LT, Lu YH, Fan HM, et al. Magnetic properties in alpha-MnO<sub>2</sub> doped with alkaline elements. *Sci Rep-UK.* **2015**;5:9094. PubMed PMID: WOS:000351150300007; English.
- [255] Ogata A, Komaba S, Baddour-Hadjean R, et al. Doping effects on structure and electrode performance of K-birnessite-type manganese dioxides for rechargeable lithium battery. *Electrochim Acta.* **2008**;53(7):3084–3093. DOI:10.1016/j.electacta.2007.11.038. PubMed PMID: WOS:000253804300009; English.
- [256] Ching S, Hughes SM, Gray TP, et al. Manganese oxide thin films prepared by nonaqueous sol-gel processing: preferential formation of birnessite. *Microporous Mesoporous Mater.* **2004**;76(1–3):41–49. DOI:10.1016/j.micromeso.2004.07.031. PubMed PMID: WOS:000225255100007; English.
- [257] Bach S, Pereiramos JP, Cachet C, et al. Effect of Bi-doping on the electrochemical behaviour of layered MnO<sub>2</sub> as lithium intercalation compound. *Electrochim Acta.* **1995**;40(6):785–789. DOI:10.1016/0013-4686(94)E0170-5. PubMed PMID: WOS:A1995QX23500014; English.
- [258] Matsuki K, Kamada H. Oxygen reduction electrocatalysis on some manganese oxides. *Electrochim Acta.* **1986**;31(1):13–18. DOI:10.1016/0013-4686(86)80054-8. PubMed PMID: WOS:A1986A18880002; English.
- [259] Cheng FY, Zhang TR, Zhang Y, et al. Enhancing electrocatalytic oxygen reduction on MnO<sub>2</sub> with vacancies. *Angew Chem Int Ed.* **2013**;52(9):2474–2477. DOI:10.1002/anie.201208582. PubMed PMID: WOS:000315209900014; English.
- [260] Cheng FY, Su Y, Liang J, et al. MnO<sub>2</sub>-based nanostructures as catalysts for electrochemical oxygen reduction in alkaline media†. *Chem Mater.* **2010**;22(3):898–905. PubMed PMID: WOS:000274089600034; English.
- [261] Li X, Xu N, Li H, et al. 3D hollow sphere Co<sub>3</sub>O<sub>4</sub>/MnO<sub>2</sub>-CNTs: Its high-performance bi-functional cathode catalysis and application in rechargeable zinc-air battery. *Green Energy Environ.* **2017**;2(3):316–328. DOI:10.1016/j.gee.2017.02.004.
- [262] Meng YT, Song WQ, Huang H, et al. Structure–property relationship of bifunctional MnO<sub>2</sub> nanostructures: highly efficient, ultra-stable electrochemical water oxidation and oxygen reduction reaction catalysts identified in alkaline media. *J Am Chem Soc.* **2014**;136(32):11452–11464. PubMed PMID: WOS:000340442700043; English.
- [263] Wang X, Yang Z, Zhang Y, et al. Palygorskite hybridized carbon nanocomposite as PtRu/r support for the methanol oxidation reaction. *Fuel Cells.* **2014**;14(1):42–48. PubMed PMID: WOS:000331904000016; English.
- [264] Yu SP, Liu RT, Yang WS, et al. Synthesis and electrocatalytic performance of MnO<sub>2</sub>-promoted Ag@Pt/MWCNT electrocatalysts for oxygen reduction reaction. *J Mater Chem A.* **2014**;2(15):5371–5378. PubMed PMID: WOS:000333101600026; English.
- [265] Ray C, Dutta S, Negishi Y, et al. A new stable Pd–Mn<sub>3</sub>O<sub>4</sub> nanocomposite as an efficient electrocatalyst for the hydrogen evolution reaction. *Chem Commun.* **2016**;52(36):6095–6098. PubMed PMID: WOS:000375346500011; English.
- [266] Li ZY, Liu ZL, Liang JC, et al. Facile synthesis of Pd–Mn<sub>3</sub>O<sub>4</sub>/C as high-efficient electrocatalyst for oxygen evolution reaction. *J Mater Chem A.* **2014**;2(43):18236–18240. PubMed PMID: WOS:000344380000013; English.
- [267] Imamura S, Tsuji Y, Miyake Y, et al. Cooperative action of palladium and manganese(III) oxide in the oxidation of carbon monoxide. *J Catal.* **1995**;151(2):279–284. PubMed PMID: WOS:A1995QD23300003; English.
- [268] Huang HJ, Chen Q, He MY, et al. A ternary Pt/MnO<sub>2</sub>/graphene nanohybrid with an ultrahigh electrocatalytic activity toward methanol oxidation. *J Power Sources.* **2013**;239:189–195. PubMed PMID: WOS:000321314100026; English.
- [269] Das S, Sarnanta A, Jana S. Light-assisted synthesis of hierarchical flower-like MnO<sub>2</sub> nanocomposites with solar light induced enhanced photocatalytic activity. *ACS Sustain Chem Eng.* **2017**;5(10):9086–9094. PubMed PMID: WOS:000412382700066; English.
- [270] Gorlin Y, Lassalle-Kaiser B, Benck JD, et al. In situ X-ray absorption spectroscopy investigation of a bifunctional manganese oxide catalyst with high activity for electrochemical water oxidation and oxygen reduction. *J Am Chem Soc.* **2013**;135(23):8525–8534. DOI:10.1021/ja3104632. PubMed PMID: WOS:000320483900022; English.
- [271] Fillaux F, Cachet C, Parker SF, et al. Inelastic neutron scattering studies of the proton dynamics in bi-doped manganese oxides. *J Electrochem Soc.* **2000**;147(11):4184–4188. DOI:10.1149/1.1394038. PubMed PMID: ISI:000090053700033; English.
- [272] Amalraj SF, Aurbach D. The use of in situ techniques in R&D of Li and Mg rechargeable batteries. *J Solid State Electrochem.* **2011**;15(5):877–890. DOI:10.1007/s10008-011-1324-9. PubMed PMID: ISI:000290040500003; English.
- [273] Shin J, Kim M, Cirera J, et al. MIL-101(Fe) as a lithium-ion battery electrode material: a relaxation and intercalation mechanism during lithium insertion. *J Mater Chem A.* **2015**;3(8):4738–4744. PubMed PMID: WOS:000349667700075; English.
- [274] Yoon HJ, Xu AR, Sterbinsky GE, et al. In situ non-aqueous nucleation and growth of next generation rare-earth-free permanent magnets. *Phys Chem Chem Phys.* **2015**;17(2):1070–1076. DOI:10.1039/c4cp04451g. PubMed PMID: ISI:000346236000040; English.
- [275] Woo SI, Kim KW, Cho HY, et al. Current status of combinatorial and high-throughput methods for

- discovering new materials and catalysts. *Qsar Comb Sci.* **2005**;24(1):138–154. DOI:10.1002/qsar.200420061. PubMed PMID: ISI:000227616700016; English.
- [276] Saal JE, Kirklin S, Aykol M, et al. Materials design and discovery with high-throughput density functional theory: the open quantum materials database (OQMD). *JOM.* **2013**;65(11):1501–1509. PubMed PMID: WOS:000327496400020; English.
- [277] Koyama M, Tsuboi H, Endou A, et al. Combinatorial computational chemistry approach for materials design: applications in deNO<sub>x</sub> catalysis, Fischer-Tropsch synthesis, lanthanoid complex, and lithium ion secondary battery. *Comb Chem High Throughput Screen.* **2007**;10(2):99–110. DOI:10.2174/138620707779940974. PubMed PMID: ISI:000244880300003; English.
- [278] Kafizas A, Parkin IP. Inorganic thin-film combinatorial studies for rapidly optimising functional properties. *Chem Soc Rev.* **2012**;41(2):738–781. DOI:10.1039/c1cs15178a. PubMed PMID: ISI:000298854900014; English.